



MICRONIC MYDATA

In-Machine Planarity Measurements of a Large Micro Mirror Array

Hanna Al-Maawali

Master of Science Thesis
KTH



KTH Engineering Sciences

Supervisor: Peter Björnängen
Examiner: Fredrik Laurell

2013-06-14

TRITA-FYS 2013:39
ISSN 0280-316X
ISRN KTH/FYS/--13:39—SE

Abstract

This work investigates if the global planarity of a spatial light modulator, SLM, installed in a laser direct imaging machine can be measured using an in-machine camera with little or no alteration to the current optical system.

In the machine there exists a camera that sees the same image of the SLM that the photosensitive substrate sees. This camera was the in-machine camera used in this work.

The planarity measured was limited to three different aspects of the planarity; the bow of the SLM in the short direction and in the long direction as well as the twist of the SLM in the short direction of the SLM.

The bow in the short direction gives a focus error at the substrate. It was measured by taking several images of the SLM through focus to determine the best focus position for the whole SLM length. The best focus position was determined by doing a Gaussian fit to the illumination in the short direction and finding the focus position at which this Gaussian illumination curve had the smallest full width half maximum, FWHM.

The twist of the SLM in the short direction gives a displacement error of the SLM image at the substrate. Images were taken of the SLM in focus and the movement of the Gaussian illumination peak was tracked. This gave the displacement error in the camera image due to the twist of the SLM.

The bow of the SLM in the long direction will give a scale error at the panel. To image this planarity, a lens was inserted imaging the Fourier plane to the camera. A small portion of the SLM was illuminated and this portion was moved downwards along the length of the SLM. In the Fourier plane, seven Fourier lines were visible. The movement of these lines was tracked and was then calculated back to the bow present on the SLM.

Both the bow of the SLM in the short direction and the twist of the SLM in the short direction seemed to be imaged well in the camera, although the optical aberrations from the system were not removed. These aberrations should be characterized and removed from the results to get a better correlation to the SLM planarity.

The bow of the SLM in the long direction could only be measured in one machine and showed some correlation with the only other data available for this planarity. More measurements need to be done to be able to tell if this is a good way to image this planarity or not.

Acknowledgements

I would like to thank the whole team of people working with the LDI machine at Micronic Mydata who have been very helpful to me during this project. There are some I would especially like to thank.

I would like to thank my supervisor Peter Björnängen and for all his support and for giving me the opportunity to do this project. I would also like to thank Andreas Bergström for all his help and insight into the workings of the SLM and Per Askebjør whose knowledge and previous work made this project possible.

I would like to thank Sten Lindau and Andrzej Karawajczyk for helping me with understanding the optics in the LDI machine.

I would like to thank Jukka Vedenpää, Ola Jacobsson, Robin Goodoree, Stefan Nilsson, Jens Regild, Johan Densjö, Artur Ginszt, Mattias Ström and Martin Camacho for all their help operating the LDI machines in the cleanroom.

I would like to thank Mikael Blomström with helping me make components for my experiments with the machines.

I would like to thank John-Oscar Larsson for helping me with octave scripts and Anders Svensson for providing me with measurements to compare to and helping me with some MATLAB issues.

Table of contents

Abstract	2
Acknowledgements	3
Introduction	5
Background	5
Aim	8
Global planarity	9
Measurement of p_2 planarity	12
Measurement of p_1 planarity	26
Measurement of T planarity	33
Conclusion and Future Work.....	43
References	44

Introduction

Micronic Mydata AB is a company that specializes in making mask writers for displays and semiconductors as well as a set of SMT solutions that include pick and place machines and jet printers. Their most recent addition is a new laser direct imaging machine, LDI. This machine writes patterns directly onto a substrate coated with a photosensitive resist instead of writing the pattern on a mask.

The LDI directs a UV-laser onto a photosensitive substrate via a spatial light modulator, SLM, to print a given pattern onto the substrate. The spatial light modulator is made up of an array of millions of micro mirrors. Each row of mirrors can be deflected differently depending on the pattern to be printed. The light reflected from the SLM is then imaged onto the substrate via a rotor arm that is swept across the surface of the substrate in a circular motion.

The precision of the writing process is determined by several factors in the machine, including alignment and quality of optics among many others. If the errors in the different components are not eliminated, the precision of the machine will not be as high as the market demands. Some of these factors cannot be eliminated by simply producing better lenses and therefore the machine measures the combined placement and focus errors from all the optical components and compensates for the flaws in the system as it writes. One contributor to the placement and focus error is the global planarity of the SLM chip in the machine.

With a way to measure the global planarity of the SLM inside the machine, it will be possible to have long term measurements on the global planarity. It will make it possible to see if the shape changes over time. If so, it will then be interesting to see how it changes over time and if it goes outside the global planarity specifications that have been set and if it then decreases the writing quality.

Being able to measure the planarity of the SLM in the machine would provide an easier way to error check the machine without having to remove it from the machine, in the case of a malfunctioning machine. This would give an indication as to whether it is the cause of the error or not without the need to remove it first.

Background

The LDI draws patterns creating printed circuit boards using a UV-laser. To understand the significance of the global planarity of the SLM chip, some information on how the machine works is needed.

LDI writing principle

The machine starts with measuring the topography of the substrate. This information, along with the desired pattern to be drawn onto the substrate, is fed into the machine. Each rotor arm gives a different placement error of the pattern and each of the four arms placement errors have been measured. With this information, the machine can write the pattern compensating for most of the placement errors to give a pattern that resembles the desired one as closely as possible. The irregularities on the surface are also compensated for by changing the focus position of the laser beam.

To write the pattern, a rotor arm will be swept across the surface of the substrate in a circular motion. A laser beam is focused onto the substrate through the rotor arm. This laser beam will change shape and a focus actuator will elongate and shorten the optical path length which changes the focus position of the laser beam to compensate for the irregularities present at the substrate surface. At the same time that the rotor is swept across the surface, the substrate is moved downwards until the whole pattern has been drawn. This writing process is shown in the sketch in Figure 1.

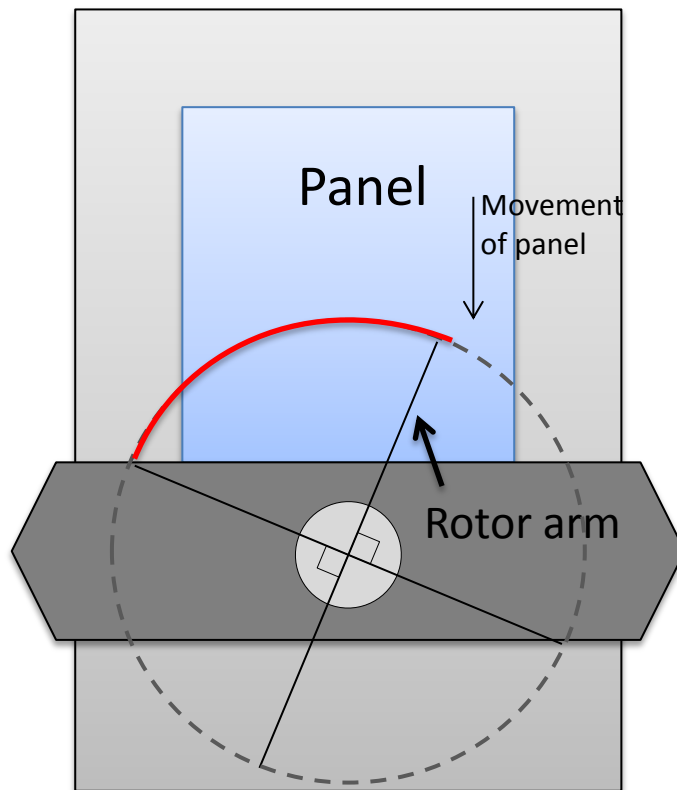


Figure 1 – A sketch of the machine showing the panel movement and the rotor movement across the panel. There are four rotor arms that make it possible to write continuously until the whole panel has been written. The laser is only focused into the arm that is currently on top of the panel.

From the laser to the rotor arm there exists a large optical system that images and alters the properties of the original laser beam to acquire the desired properties necessary to be able to write properly. The laser beam is first corrected to obtain a good quality beam. This beam is then imaged onto the SLM chip surface. The SLM chip is in turn imaged onto the substrate surface. The first optical system imaging the laser beam onto the SLM is described below.

The laser beam is divided into nine lines. Each line illuminates the whole SLM chip surface. These lines make it possible to illuminate the length of the SLM making sure that each part of the SLM sees both strong and weak parts of the original beam (peak and tails of Gaussian illumination respectively). The illumination is shown in Figure 2.

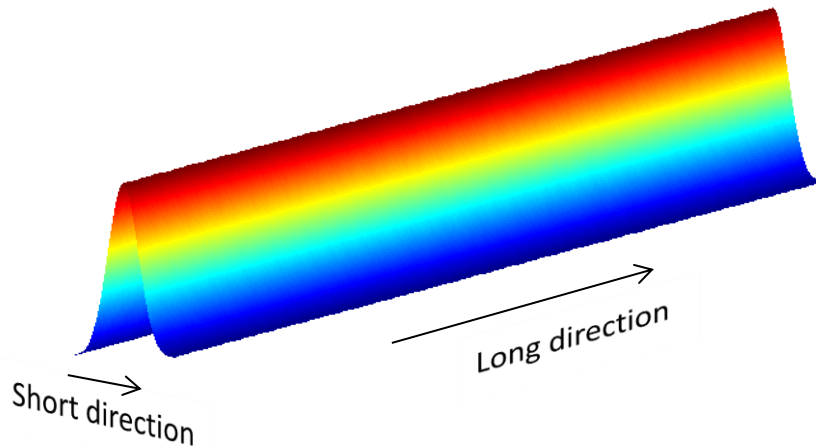


Figure 2 – The illumination on the SLM gives a top-hat illumination along the long direction of the SLM and a Gaussian illumination along the short direction of the SLM [1].

The SLM is then imaged onto the substrate via a second optical system. This part rescales the SLM so that the image on the substrate is smaller. The system can be replaced by two lenses and is illustrated in Figure 3. The actual system contains several more lens elements necessary to decrease aberrations in the optics.

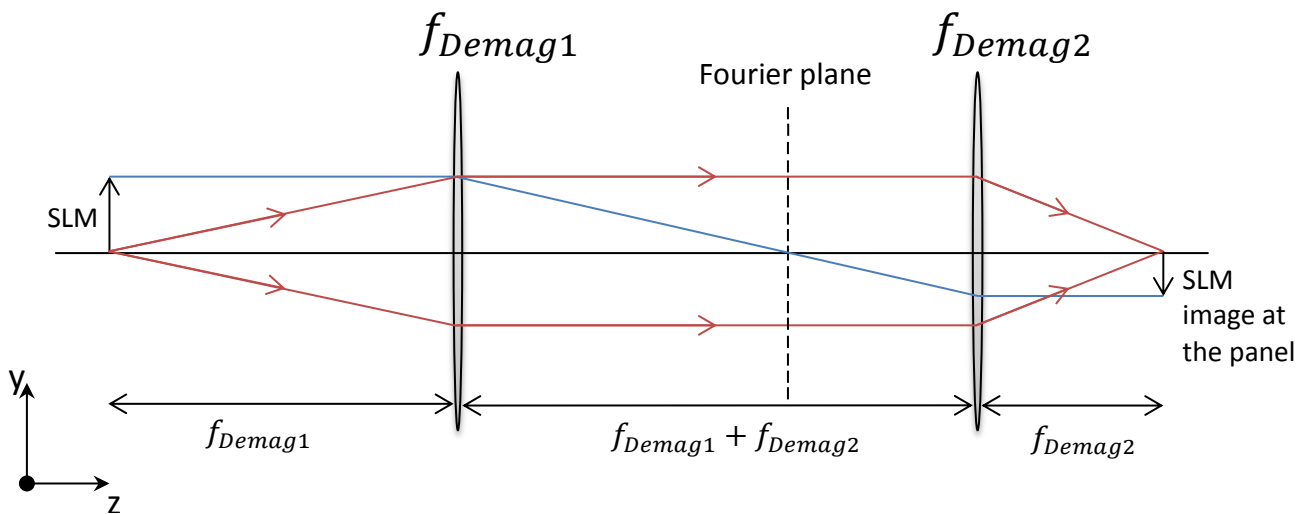


Figure 3 - A schematic view of the optical system from the SLM to the panel. The Fourier plane lies at the back focal point of the first lens and the front focal point of the second lens. The y-direction corresponds to the long direction of the SLM and the x-direction corresponds to the short direction of the SLM.

Figure 3 shows that the SLM is placed at the focal distance f_{Demag1} from the first lens. The second lens is then placed at a distance $f_{Demag1} + f_{Demag2}$. This creates a telescopic system where rays parallel to the optical axis entering the first lens will exit the second lens also parallel to the optical axis. A full description of the projection optics showing the projection of the SLM image to the panel can be found in [2].

Since the SLM is effectively imaged onto the substrate, the planarity of the SLM will directly affect the writing quality of the LDI machine.

The SLM chip

The SLM is made up of an array of millions of micro mirrors (Optical MEMS). These mirrors are built up on a large piece of silicon wafer. This SLM chip is then glued onto a piece of a ceramic material that has similar thermal properties [3].

Each row of mirrors is assigned as a pixel. This means that each row of mirrors can be controlled individually. When the mirrors are deflected slightly, they will diffract the reflected light. The more the mirrors are deflected, the more the light is diffracted. When the light is diffracted a central peak is present with a number of outlying peaks of smaller intensity [4]. When the light is diffracted more, the intensity of the central peak decreases and the intensity of the outlying peaks increases. Once all the illumination is diffracted from the central peak to the outlying peaks, no illumination will reach the panel. This makes it possible to have a grayscale imaging process which increases the precision of the edge position of the pattern to much higher than the SLM pixel resolution.

The planarity of the SLM is currently measured at the Fraunhofer-Institut für Photonische Mikrosysteme IPMS in Germany using a white light interferometer. Only the SLMs that pass the planarity requirements are shipped over to Sweden to be installed into a LDI machine.

The planarity is also measured indirectly by measuring the errors that are present in a printed pattern. This pattern will however be the sum of all errors present in the machine. More information on how this measurement is done can be found in [5].

Aim

The aim of this master thesis project is to measure the planarity of the SLM after it has been installed into the machine, using the existing in-machine camera. The solution is supposed to be simple, in the way that the current optical system should not need to be altered too much. The measurement could tell a user whether the SLM chip is the cause of a malfunctioning machine or not, as well as permit long-term measurements of the SLM planarity.

Global planarity

In this work, the planarity measurements have been limited to studying three different aspects of the global planarity. These will be measured separately. The following text will explain how these aspects are defined and what type of writing error they will contribute to.

The first aspect of the planarity is the bow in the short direction of the SLM. This is shown in Figure 4. The bow in the short direction is given by the radius of curvature of the SLM, $R_{curv,x}$, in the short direction relative to the x-axis. The parameter that describes it is defined as p_2 and is proportional to two times the inverse of the radius of curvature.

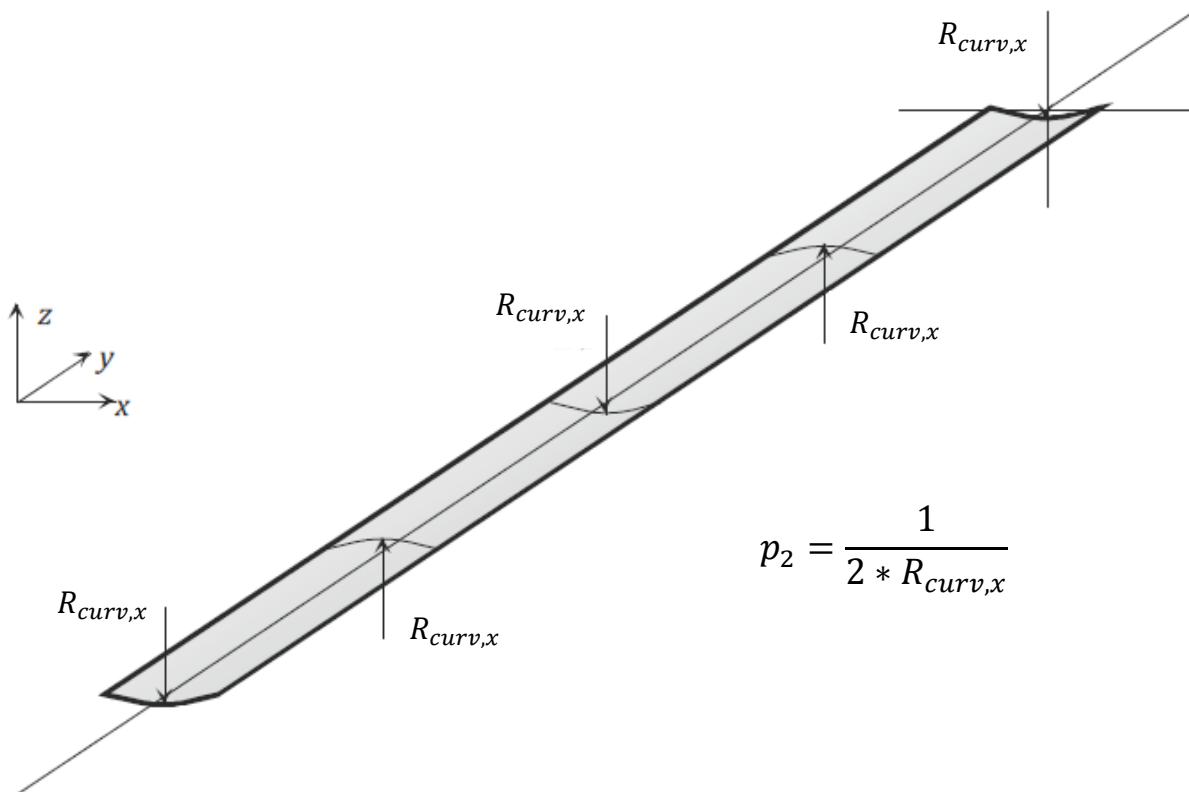


Figure 4 - A sketch showing the bow of the SLM in the short direction. The relation between p_2 and the radius of curvature of the SLM is also shown [6].

If the SLM was completely flat, the radius would approach infinity and p_2 would approach zero. With a radius smaller than infinity, p_2 greater than zero, the SLM would give a focus error at the panel. This means that with a varying radius along the length of the SLM, the focus for the different parts of the SLM will not be the same. The image of the SLM at the panel will then be sharp at some places and blurry at others. A sketch in Figure 5 illustrates the image defects that could be present on an SLM that has a curvature in the short direction.

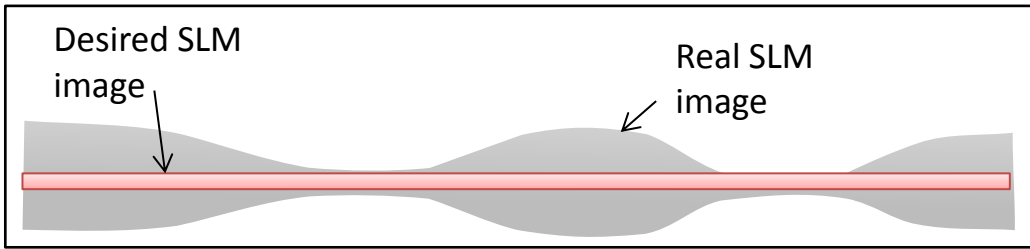


Figure 5 – A sketch showing what image effects could be present due to the bow of the SLM in the short direction. A sketch of the desired image is shown for comparison.

The machine can only compensate for a common bow in the short direction. This means that a varying radius of curvature will not fully be compensated for.

Since the real SLM image will not always be completely in focus for the whole length of the SLM, the machine will write in the best focus when it is writing “in focus”. The best focus position is the position at which the SLM image has the least possible amount of focus error for a given SLM chip. Through the rest of this report, the in focus position will refer to this best focus position.

The second aspect is the twist of the SLM. The twist is defined through the angle p_1 that the SLM makes with the x-axis, as displayed in Figure 6 below.

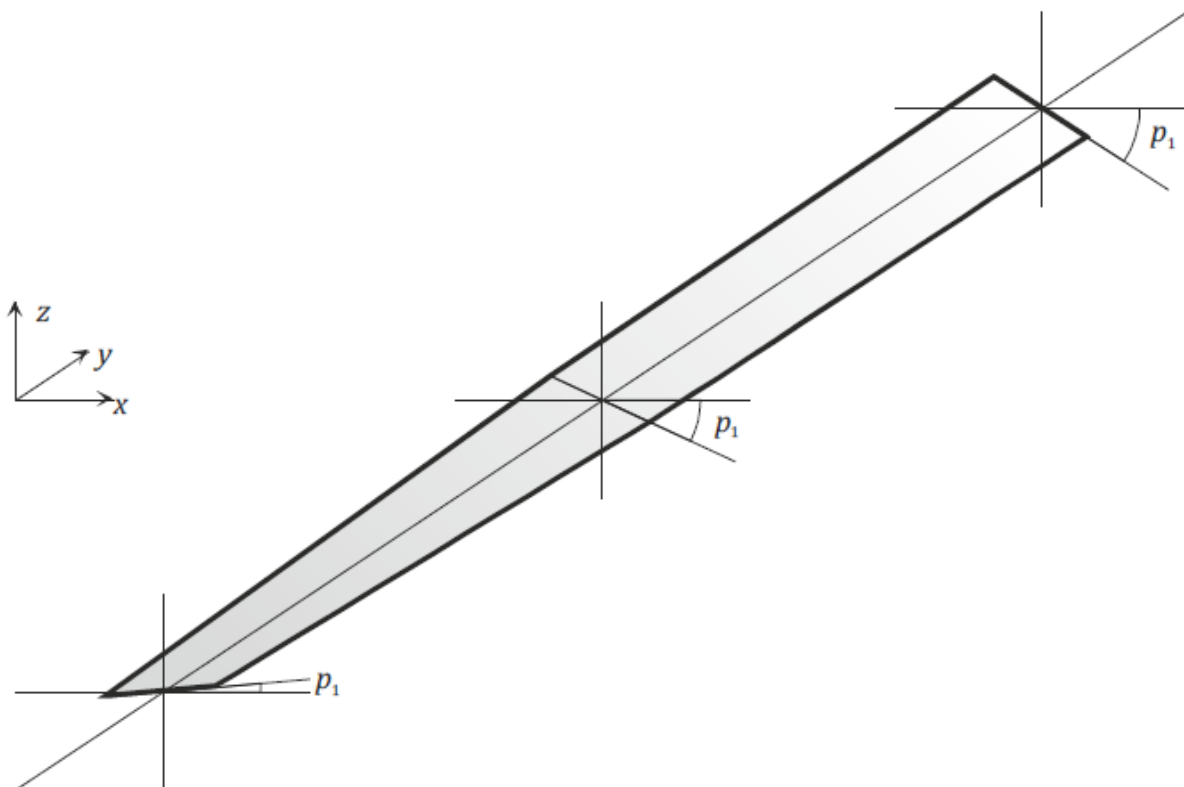


Figure 6 – A sketch of the twist of the bow in the short direction showing the angle p_1 that is made to the x-axis of the SLM [6].

If the SLM was completely flat this angle would be zero. If the SLM has a twist, such as the one in Figure 6, the image of the SLM at the panel will be crooked instead of being a straight line. This will give a placement error of the pattern. The crookedness can be compensated for

quite well with the writing algorithm. The placement error is sketched in Figure 7. The placement error is referred to as δx in the figure.

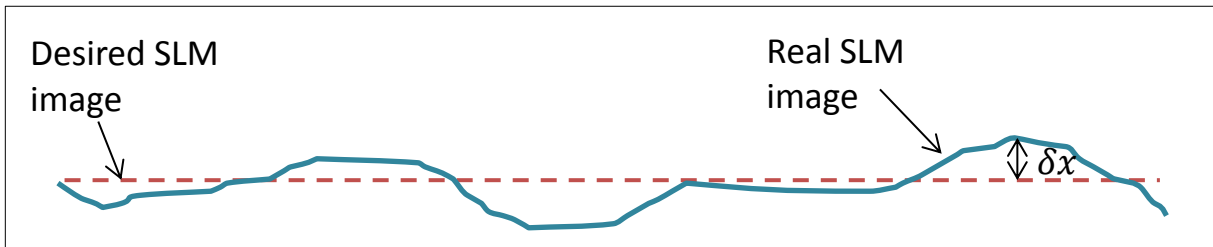


Figure 7 – A sketch showing the possible image defects that can occur when the SLM has a varying p_1 angle. The dashed line represents the desired image and the solid line represents the image due to the angle p_1 that the SLM makes with the x-axis.

The third aspect of the planarity is the bow of the SLM in the long direction. This is given by the angle T that the SLM makes with the y-axis (long direction), Figure 8.



Figure 8 – A sketch of the bow in the long direction of the SLM. The x-axis is now going into the figure, so the SLM has been turned onto its edge in the sketch [6].

The bow in the long direction will give a scale error at the panel when the machine writes out of focus. This scale error is due to the fact that the SLM image at the panel will be longer or shorter depending on the focus position. This will be the same as a placement error of a pattern in the y-direction. As for the bow in the short direction, a common bow in the long direction can be compensated for.

Measurement of p_2 planarity

In the machine there exists a camera which is placed so that it sees the same SLM image as the panel does. This means that the SLM image at the panel in Figure 3 can be replaced by the SLM image in the camera plane. By moving the camera through focus, i.e. changing the z-position of the camera, the z-position which gives the best focus can be determined for each part of the SLM. This will make it possible to determine the bow in the short direction, p_2 planarity, since this gives a focus error at the panel and therefor gives a focus error on the camera.

A curved SLM can be seen as a mirror with a radius of curvature R. A parallel incoming beam will focus the beam to a spot $f=R/2$ in front of the mirror. A typical mirror is shown in Figure 9 with the focus indicated.

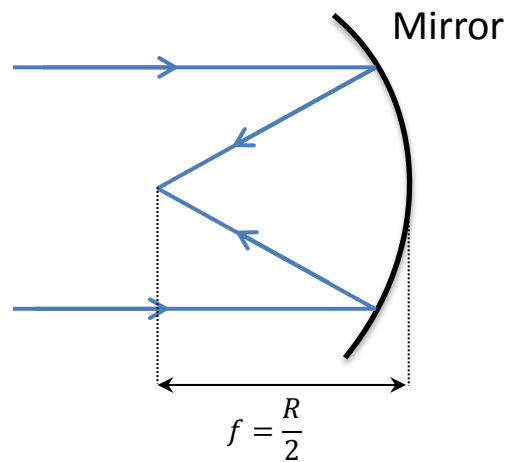


Figure 9 – Parallel beam incident of a curved mirror with radius of curvature R.

The SLM can almost be seen as the curved mirror in Figure 9. The difference is that the beam has a reversed propagation, meaning that the beam will be parallel after reflection off the mirror. The SLM is placed at a distance z_{illum} from the illuminator focus to create a wider illumination on the SLM. This will also give a virtual focus behind the SLM. The illumination on the SLM is illustrated in Figure 10.

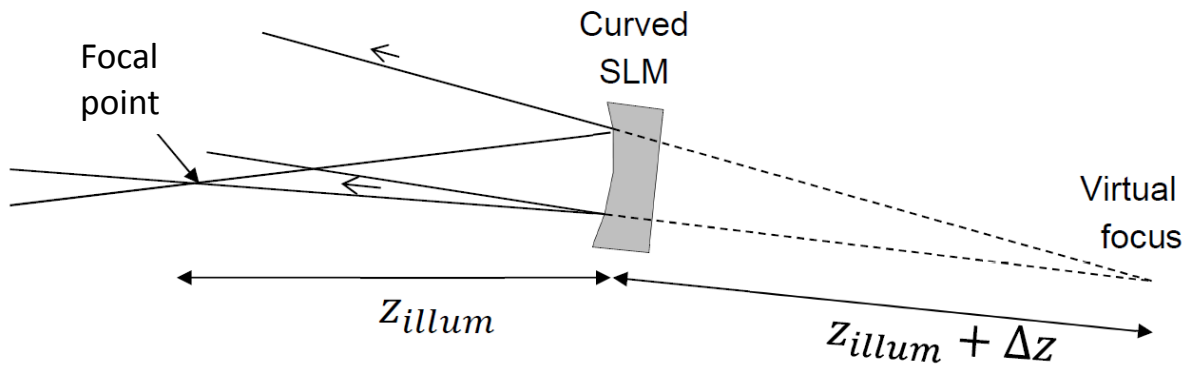


Figure 10 – Illumination of the SLM showing a wider illumination on the SLM and the position of the virtual focus due to the curvature of the SLM [1].

The distance from the focal point and the SLM surface has been denoted z_{illum} . The distance from the SLM surface to the virtual focus will then be $z_{illum} + \Delta z$, Δz being the focus error that the curvature of the SLM will contribute to. By putting these distances into the lens makers' formula, a relationship between the curvature of the SLM and the contributing focus error can be established as follows:

$$\begin{aligned} \frac{2}{R} &= \frac{1}{z_{illum}} - \frac{1}{z_{illum} + \Delta z} \Rightarrow \frac{2}{R} = \frac{z_{illum} + \Delta z - z_{illum}}{z_{illum}^2 + z_{illum}\Delta z} \\ \{z_{illum}\Delta z \text{ is small}\} &\Rightarrow \frac{2}{R} = \frac{\Delta z}{z_{illum}^2} \\ \Rightarrow R &= \frac{2z_{illum}^2}{\Delta z} \end{aligned} \quad (1)$$

Since the focus is virtual, the distance to the focus will be negative in the lens makers' formula, hence the minus sign at the beginning of the calculations [7]. The term $z_{illum}\Delta z$ is assumed to be small in comparison with z_{illum}^2 and is therefore eliminated from the denominator in the calculations.

From the SLM to the camera there exists an optical system which magnifies the image by a factor M . Since the focus shift will be along the optical axis, the lateral magnification will be M^2 [7]. To be able to get the relation between the radius of the SLM and the shift in focus in the camera plane, equation (1) needs to be multiplied by this factor. This gives the equation:

$$R = \frac{2z_{illum}^2 * M^2}{\Delta z} \quad (2)$$

The equation shows that if Δz approaches zero, then R approaches infinity, giving a flat surface. Using the equation in Figure 4 together with equation (2) a relationship between the focus shift and the parameter p_2 can be determined.

$$\begin{aligned} p_2 &= \frac{1}{2R} = \frac{\Delta z}{4z_{illum}^2 * M^2} \\ \Rightarrow \Delta z &= 4 * z_{illum}^2 * M^2 * p_2 \end{aligned} \quad (3)$$

Experiment

The SLM was fully illuminated with the mirrors non-deflected so that they reflected as much light as possible; they were set to "white". The camera was moved 100 μ m out of focus in both directions of the propagation direction of the beam, z-direction, with a focus step of 4 μ m. The camera used does not cover the whole SLM in one image and therefore three images were taken of the SLM to cover the length of the SLM. This gave a total of 153 images, 51 images for each of the three camera positions. Images were taken with a pulse pattern to be able to identify at which camera pixel the images should be stitched together. To eliminate background noise, a picture was also taken with the laser shutters closed for each of the camera positions.

The focus range that the curved SLM will contribute to is expected to be smaller than the 200 μ m that the camera has been moved. This extra-large range is due to a tilt of the camera. The camera tilt will then exaggerate the distance which the camera needs to be moved.

This measurement and the coming analysis were done on two machines and hence two different SLM chips.

Analysis

Each set of images from each camera position were analyzed individually and then stitched together at the end of the analysis. All of the images were loaded into MATLAB and the background noise was subtracted from all images. One set of images for a focus position is displayed in Figure 11.

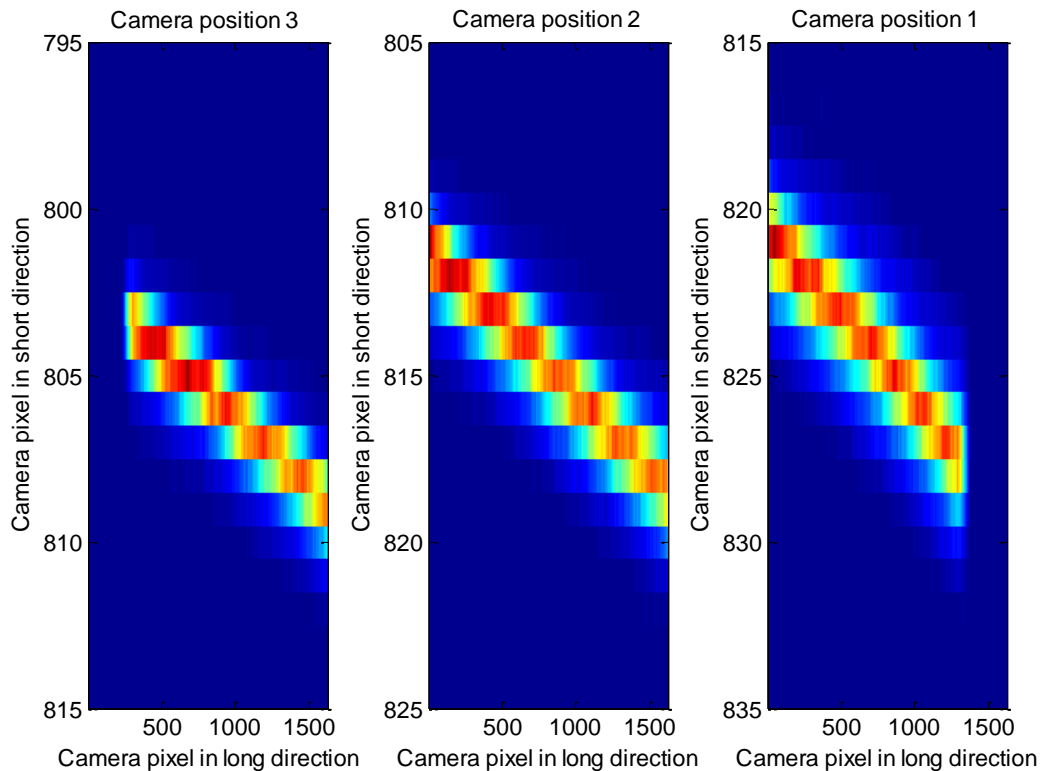


Figure 11 – A set of images for a z-position showing a slanting SLM image for all three camera position.

These images show that the SLM image was not aligned with the pixel array of the camera. Before any analysis was done, the images were rotated to form a straight SLM image. The images also cover a larger area than that used by the SLM. To identify the end pixels in the images at position 1 and 3, the pulse pattern was utilized.

The pulse pattern is designed so that two sets of mirror pixels are tilted white with a set number of pixels in between. This is to be able to identify the edge of the SLM in the images. In between the edge pulses there is an equidistant pattern that has the first pulse containing one set of mirror pixels set to white, and the second pulse contains two sets of mirror pixels set to white and so on. This pattern covers the length of the SLM. The profile of the three images taken at the different camera positions of the pulse pattern are displayed in Figure 12.

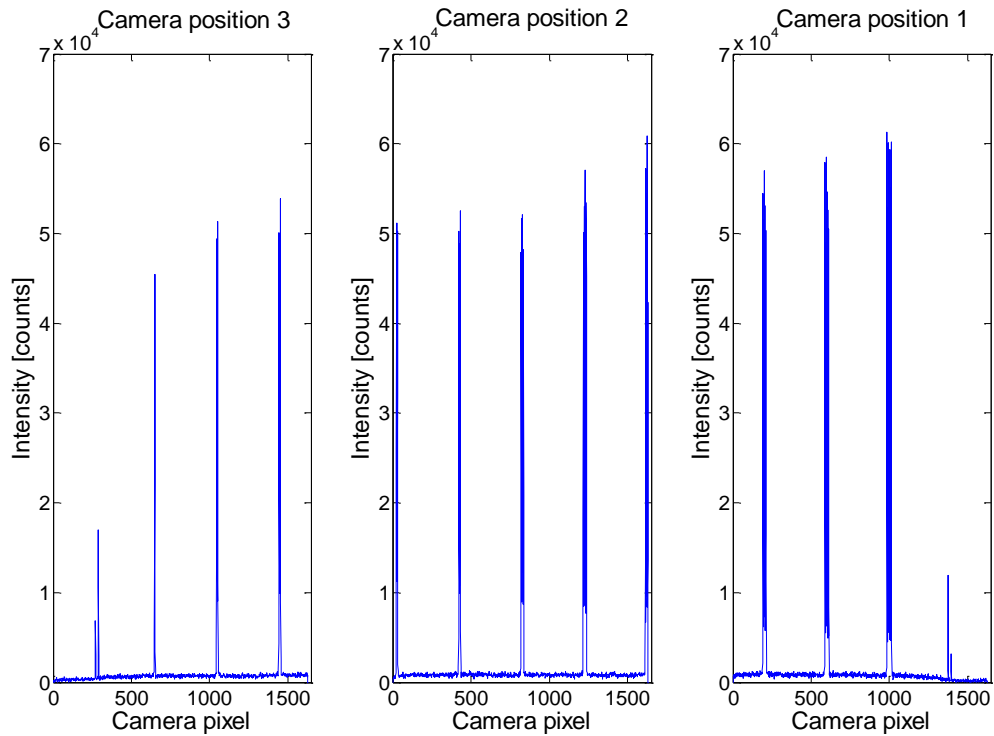


Figure 12 – Plots showing the pulse pattern in the three different camera images that are to be stitched together.

Since each set of pulses has a different amount of peaks, the pulses that have the same number of peaks in the images made it possible to identify at which camera pixel the three images should be stitched together. This corresponds to the same pixel at which the images of the completely white SLM will need to be stitched together and makes it possible to stitch the images together later on. By using this pattern to stitch together the images, the uncertainty in the position the length of the SLM will be very low (less than 10 SLM pixels).

All of the 51 images at each camera position were rotated and the images at position 1 and 3 were cropped to the first and last pixel identified in the pulse pattern. The images in Figure 11 will then look as in Figure 13.

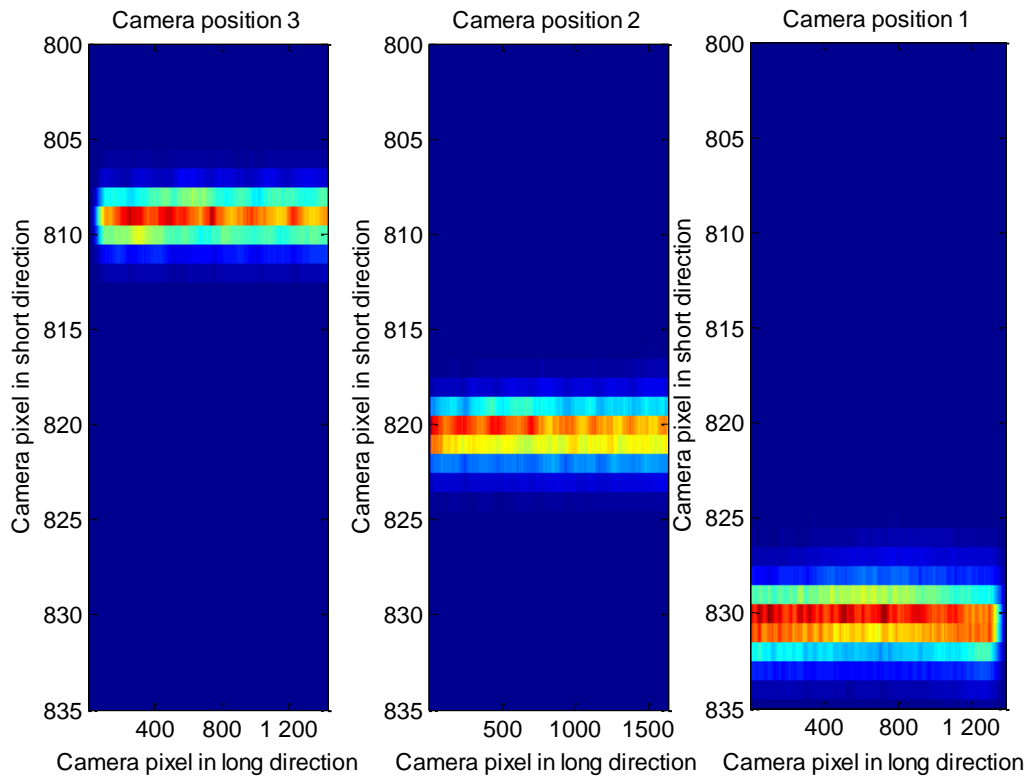


Figure 13 – The SLM image has been rotated for each camera position to ease calculations.

Even though the images at camera position 1 and 3 have been cropped to the edges of the SLM, the intensity drops rapidly at the edges. By plotting the profile of these images, Figure 14, a taper can be seen at the edges of the SLM. This taper is used as an area where the pattern is printed twice to improve the writing quality in the overlap between the rotor arm sweeps. Due to this taper, the SLM pixels hidden behind the darkest half of the taper were not included in the image analysis.

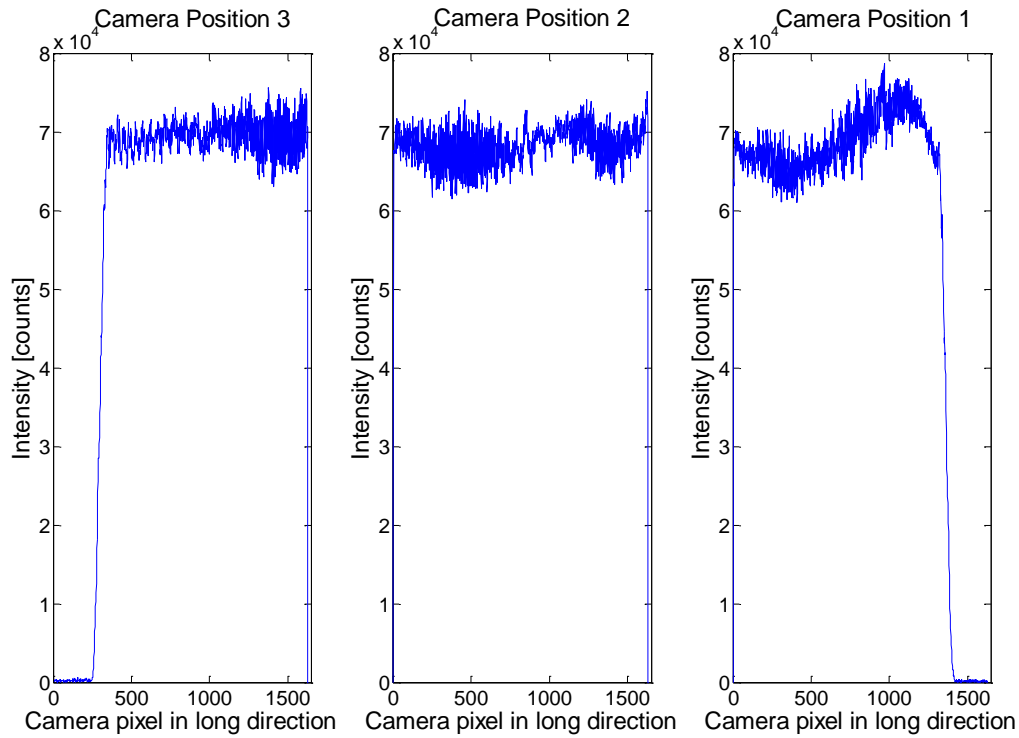


Figure 14 – Plots of the profile of the three images of the SLM. The edges of the SLM seen in camera position 1 and 3 have a taper present that makes it difficult to determine the Gaussian illumination separate from the background noise.

From the images in Figure 13, it was now possible to determine the camera position at which the best focus for each SLM pixel in the long direction can be achieved. The best focus was assumed to be at the z- position where the illumination is the narrowest in the short direction. A Gaussian fit in the short direction was done to each pixel in the long direction as in Figure 15. The width of this Gaussian fit was recorded for each pixel in the long direction and for each z-position of the camera.

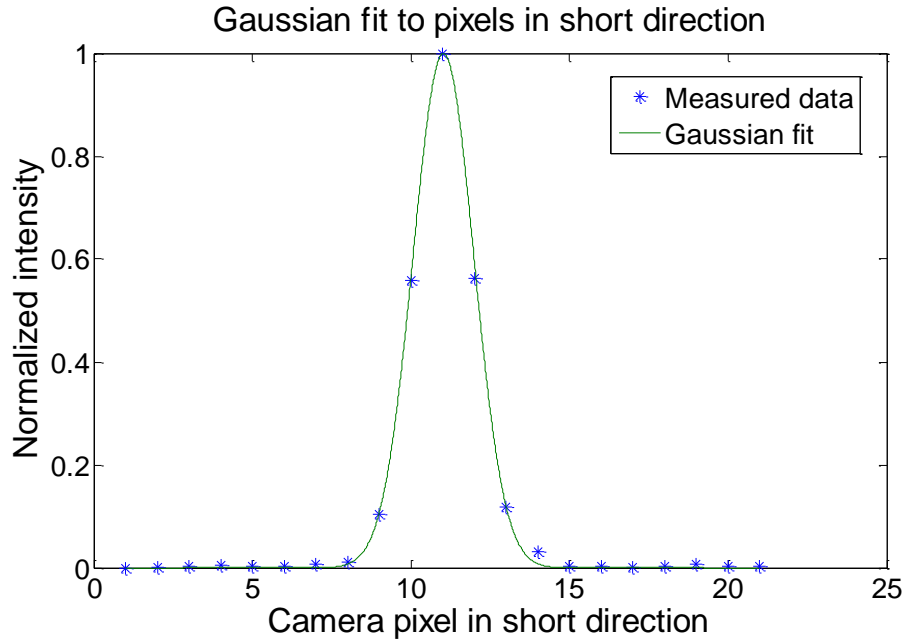


Figure 15 – A plot showing the Gaussian fit to the intensity of the SLM in the short direction.

The FWHM values of one SLM pixel for each of the focus positions, the 51 images, were then plotted and a second degree polynomial fit was done to the data points. The minimum of this polynomial fit curve then corresponds to the z-position at which this pixel has the best focus. This fit is shown in Figure 16.

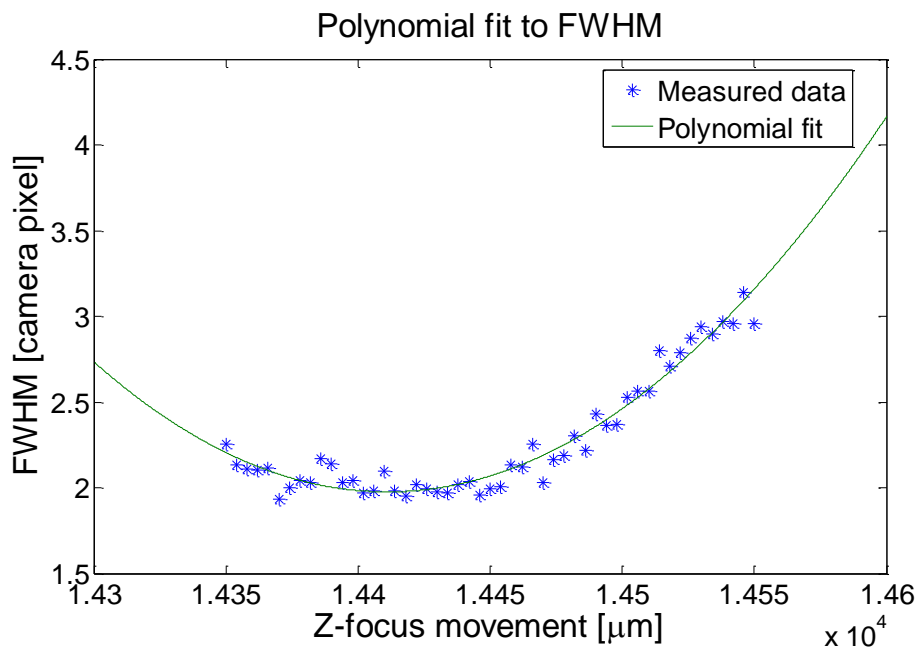


Figure 16 – A plot showing the second order polynomial fit that is done to the FWHM of the Gaussian fits to be able to determine the minimum positions that give the z-position of the camera with the best focus for each pixel in the long direction of the SLM.

The polynomial fit was done for each SLM pixel. The minimum values were recorded for the three camera positions and the data was stitched together at the positions indicated from the

pulse pattern. The resulting plot showing the movement of the focus position along the SLM is shown in Figure 17.

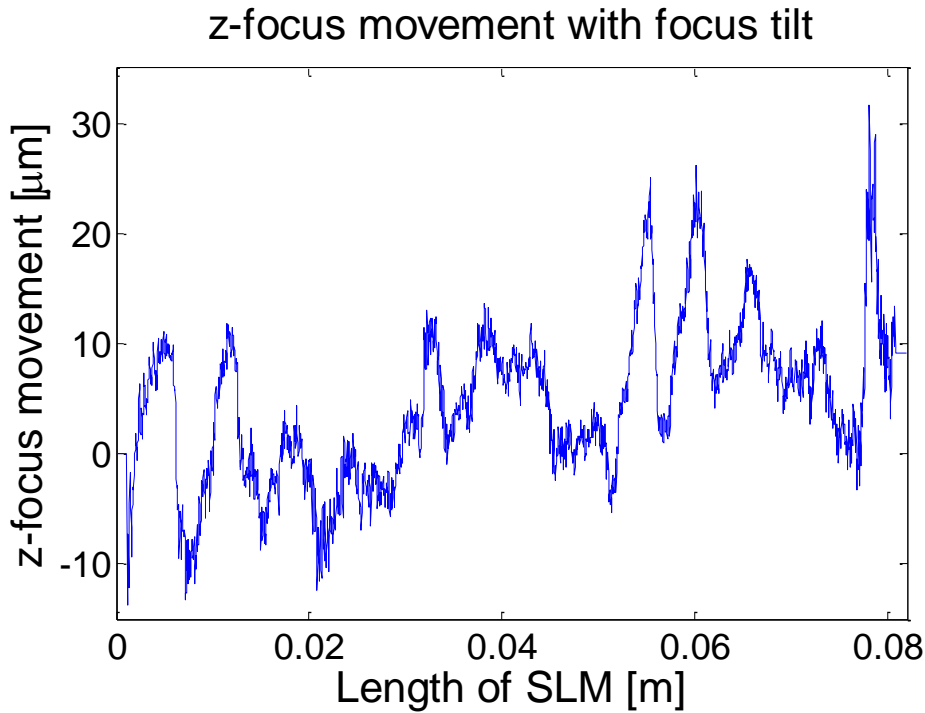


Figure 17- The z-position of the best focus showing a slight upward tilt due to the focus tilt from the SLM image plane not being orthogonal to the camera plane.

The plot in Figure 17 shows a slight upward tilt. The upward tilt is caused by the camera plane not being orthogonal to the incoming SLM image. This linear trend is removed and the resulting plot is shown in Figure 18.

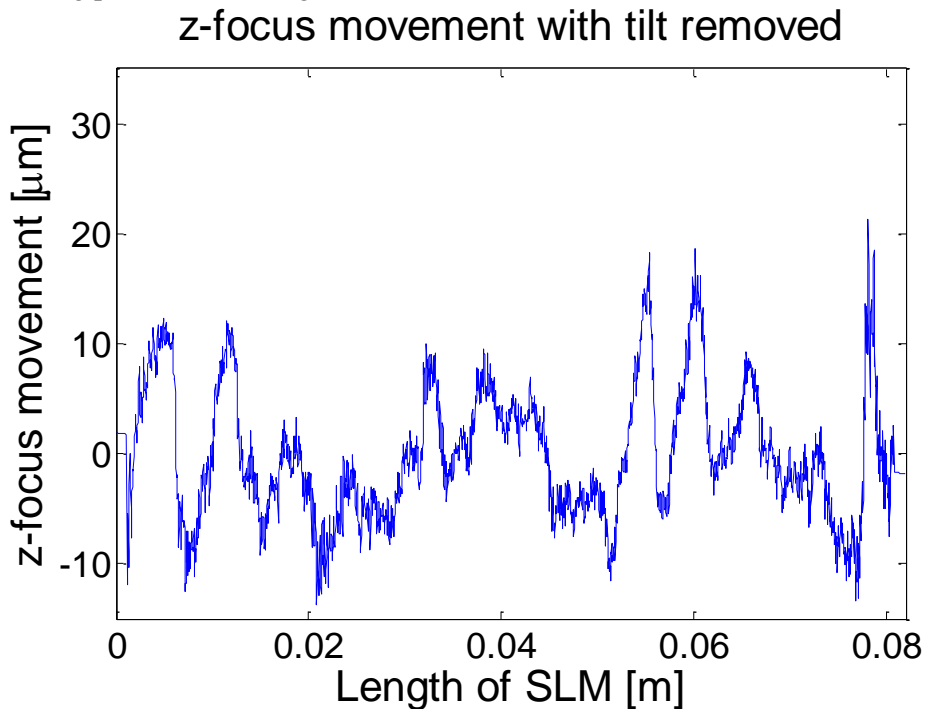


Figure 18 – The z-position of the best focus for each SLM pixel in the long direction before filtration.

The plot in Figure 18 has a periodical effect that is not a characteristic of the SLM surface. Since the original image in Figure 11 was rotated and the analysis done on the rotated image, a closer look at the un-rotated image can explain this periodicity.

The period in Figure 18 can be seen to correspond to each time the peak of the SLM hits a new camera pixel in the y-direction of Figure 11. A band stop filter was created that removes the frequency that corresponds to this period. The data was inserted into this filter and the filtered plot of Figure 18 is shown in Figure 19.

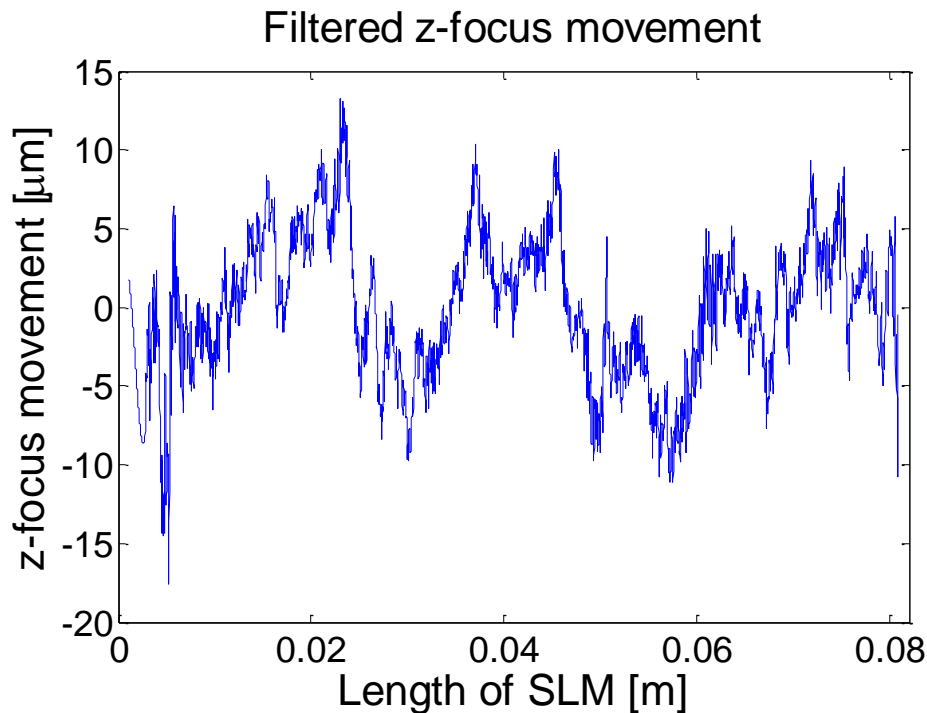


Figure 19 - The z-position of the best focus for each SLM pixel in the long direction after filtration.

The resulting plot in Figure 19 no longer has the periodical effect but it still contains quite a large amount of noise. To reduce this noise, the data was sent through a second filter which acted as a moving average filter. The moving average filter takes a measurement point and sets it to the value of the average of the previous 10 points and the 10 points after the measurement point. For the points at the edge of the plot, e.g. the first value of the plot, there does not exist 10 points prior to the value, therefore the subsequent 10 points are mirrored along the x-axis and the y-axis to create these 10 points prior to the first value. This average calculation is then done for all of the points in the plot. The resulting plot after the moving average filtration of Figure 19 is shown in Figure 20.

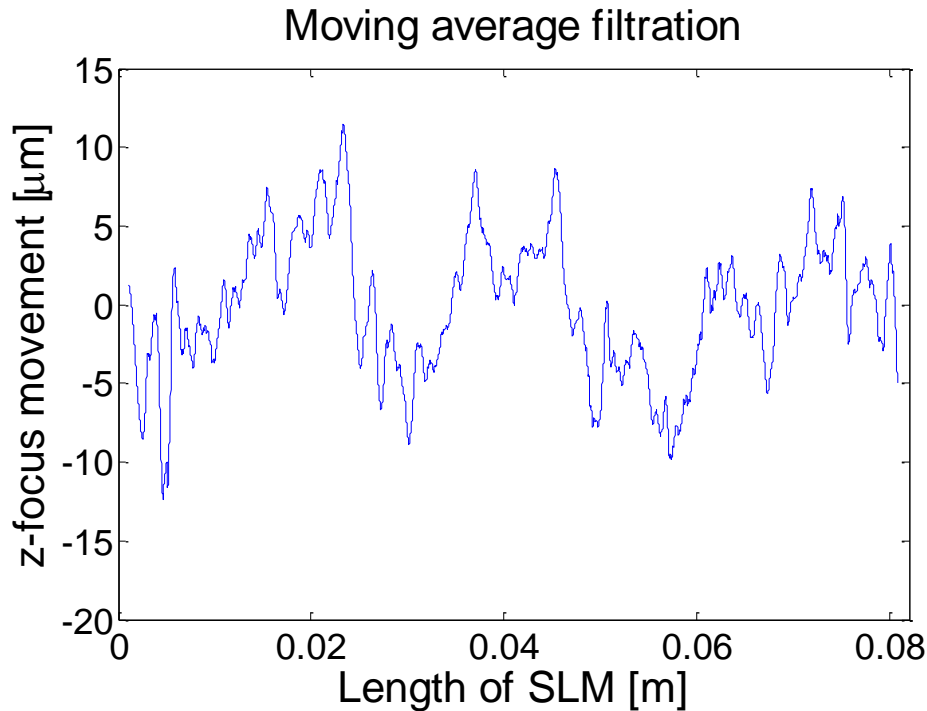


Figure 20 – The z-focus plot after it has passed through a moving average filter to minimize the noise in the plot.

The plot in Figure 20 consists of the final plot of this analysis showing the shift in the focus point along the length of the SLM. The full code used to do this image analysis can be found in [8].

Uncertainty calculations

The uncertainty of the results was determined with Monte Carlo simulations. A Monte Carlo simulation involves applying a distribution over a data set and creating a large number of random values within this distribution. The calculations are then made for all of the random values creating a large amount of final results. Taking the standard deviation of these final result values will then be the uncertainty of the final result.

To do this Monte Carlo simulation, two images were taken of the SLM at the same position. The two images were used to determine what kind of intensity noise is present in the camera. By taking one image minus the other, the difference in detected intensity was obtained. This difference was larger for a pixel that had detected a high intensity value and lower for a pixel that had detected a low intensity value.

The intensity points used in the Gaussian fit in Figure 15 were given a noise with a normal distribution that had the measured value as the mean and the difference in intensity as the standard deviation. The standard deviation was higher for the intensity points that had detected a higher intensity ($>10\,000$ counts). An amount of 1000 random values of each intensity point in Figure 15 was generated within each point's distribution. A Gaussian fit was done for these 1000 sets of random intensity values giving 1000 different FWHM values.

The same simulation described in the paragraph above was done for the same pixel in the 51 different focus positions. These 1000 different FWHM values for each of the 51 focus

positions gave an uncertainty in the y-direction of the points in the polynomial fit plot in Figure 16.

The uncertainty in the x-direction of the plot in Figure 16 is the uncertainty in the focus position. This uncertainty is approximated to $\pm 50\text{nm}$ and is assumed to have a normal distribution with the mean value as the measured value and a standard deviation of $\frac{100\text{nm}}{6} \cong 17\text{nm}$. As for the uncertainty in the FWHM values, 1000 random values within the normal distribution previously stated were generated for each z-focus movement value in Figure 16. Combining the two uncertainties for each data point in Figure 16 gave 1000 different sets of data for one pixel. A second order polynomial fit was done to each of the 1000 sets of data points. The minimum value was taken for each polynomial fit and the resulting standard deviation of all the 1000 different minimum values gave the standard deviation of the z-focus values in Figure 18. The range of the error was taken to be six standard deviations resulting in $\pm 0.57\mu\text{m}$ error for each focus value. The plot from Figure 20 is shown in Figure 21 below with this error represented as error bars.

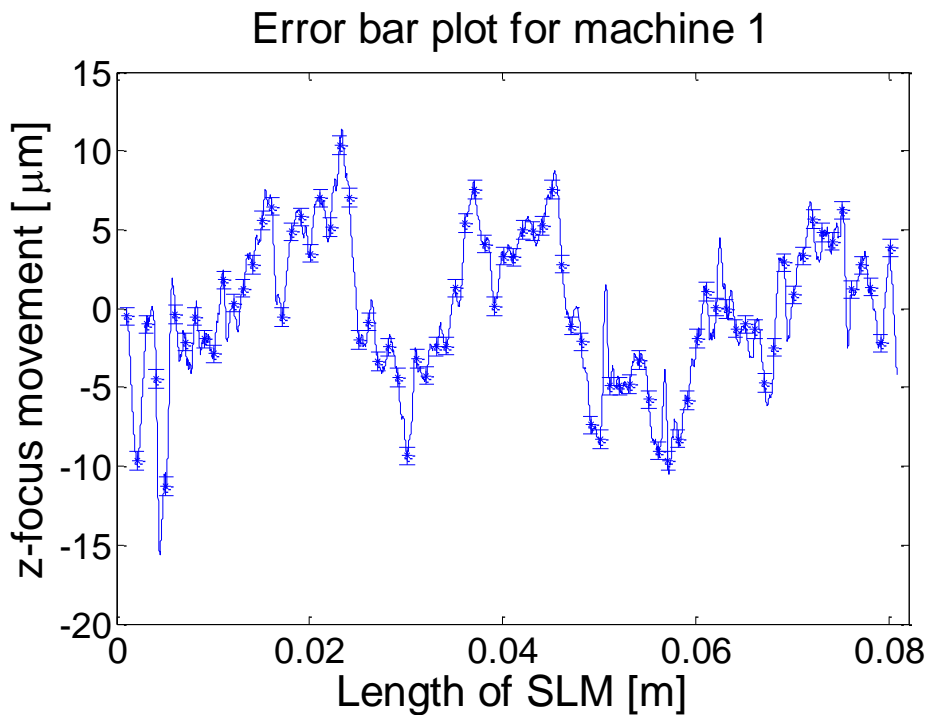


Figure 21 – Error of z-focus movement for machine 1.

Since the plot in Figure 21 consists of over 3000 data points, only every 100 data points have error bars to be able to interpret the amount of error present in the plot.

Results and Analysis

The results of the measurements and image analysis for the two machines are displayed below in comparison with the two sets of data that are available. One of them is the data from the Fraunhofer Institute prior to installation and the other one is the focus error on the panel after installation.

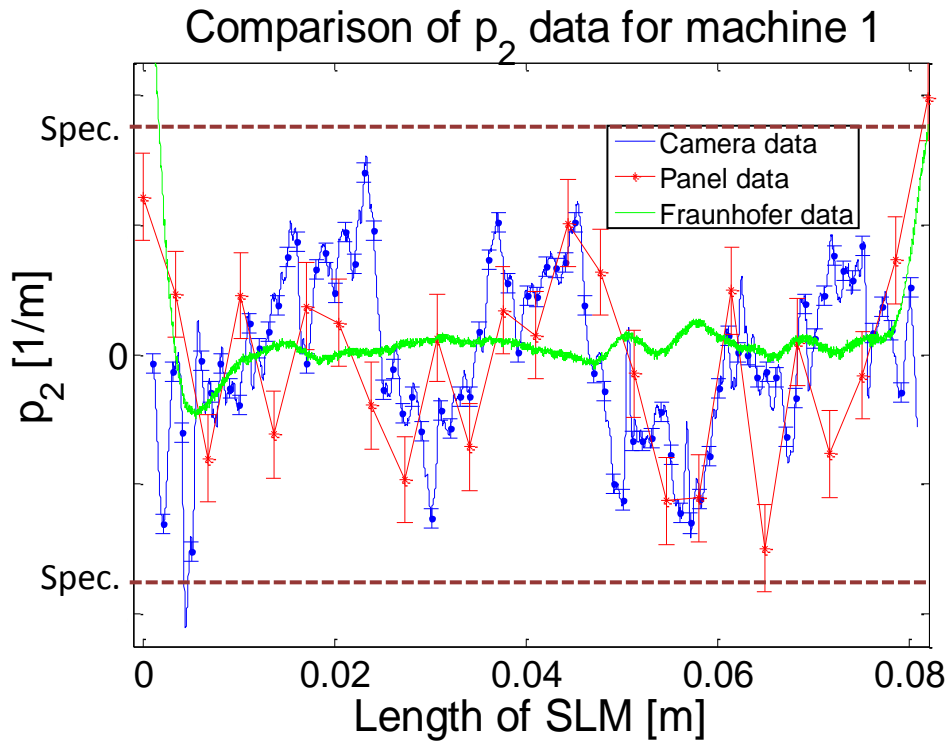


Figure 22 – A plot showing the data from machine 1 that was collected using the camera along with the other two measurements available.

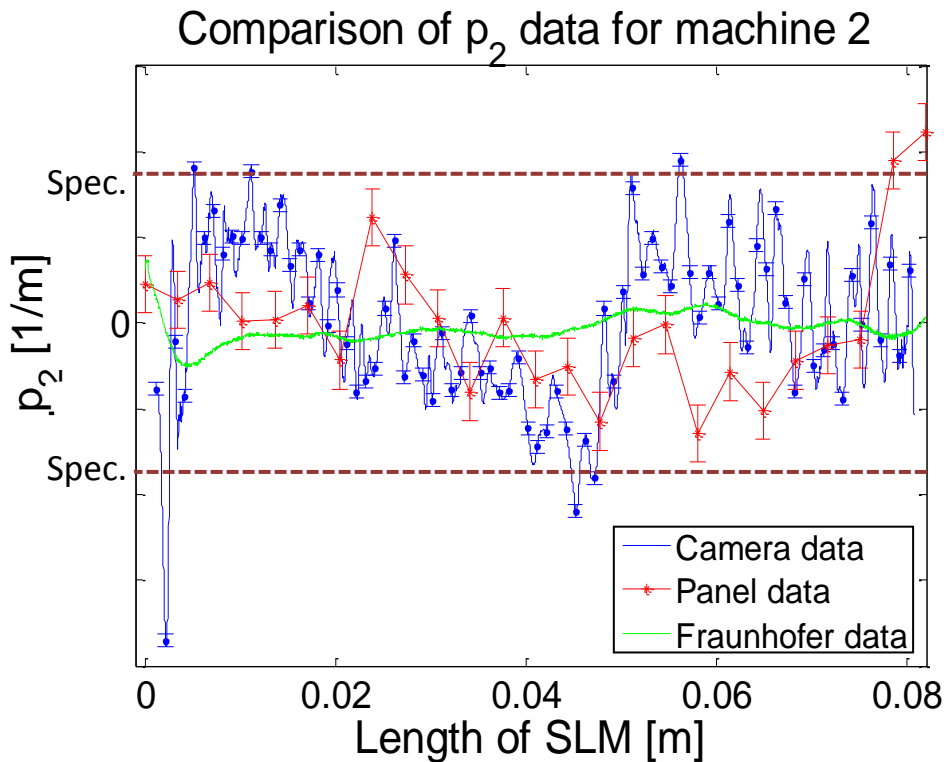


Figure 23 – A plot showing the data from machine 2 that was collected using the camera along with the two other measurements available.

Due to non-disclosure of confidential information, the values on the y-axis have been removed. The horizontal dotted lines represent the range at which the values are within range. For specification values see the acceptance values in [9].

The measurement from the camera data consists of around 3200 data points. The Fraunhofer data consists of around 4400 points which are an average of a much larger amount of measurement points, at least ten times more. On the other hand, the panel data consists of 25 data points. This means that the panel data could miss some irregularities along the SLM length in between the sampled points compared to the camera and Fraunhofer data that have data for approximately every other SLM pixel.

Since the panel data is the focus error at the panel, it means that the SLM image has travelled through more optics than the image present on the camera. These extra lenses will contribute to the focus error recorded on the panel and possibly alter the data between the camera and the panel.

The uncertainty in the camera data is less than the uncertainty approximated for the panel data. The Fraunhofer data is assumed to have an error much smaller than the variations of p_2 along the SLM and is therefore not shown in the figure.

The data displayed in Figure 22 shows a good correlation between the panel data and the camera data. The data displayed in Figure 23 does not show such a good correlation. This data has a lot of noise compared to the previous result from machine 1 and could be the reason why the correlation is so much worse. It is also possible that the optics between the camera and the panel in machine 2 are affecting the measurements more than in machine 1.

Table 1 shows how much the range of the different data sets differ from the specification range in percent. To clarify, the camera data for machine 1 exceeds the specification limit by 21% with an uncertainty of 2.1% whilst the Fraunhofer data for machine 1 has a range 13% lower than the specification limit. This is how the percentages in Table 1 have been calculated.

	Machine 1	Machine 2
Camera data	+21% \pm 2,1%	+84% \pm 2,1%
Panel data	-3,5% \pm 9,3%	-2,4% \pm 9,3%
Fraunhofer data	-13%	-79%

Table 1 – A table summarizing the difference in ranges of the p_2 data from the two machines.

The edge pixels in Figure 22 for the Fraunhofer data vary much more than the pixels in the middle region of the plot. These edge pixels were not included in the calculations for the camera data due to the taper present in Figure 14. To get a better comparison of the ranges of the data sets, the range of the Fraunhofer data is taken from approximately the same parts of the SLM as the camera has analyzed data for.

For machine 1, the camera has a range 25% larger than the panel range and has a range that exceeds the specification limit by 21%. The panel data only has 25 points and could easily have missed a variation between the points that would increase the range of the panel data. This along with the extra optics that it traverses could be an explanation to why the values differ so much.

For machine 2, the camera has a range 84% larger than the panel range. As noticed earlier, there exists a large amount of noise in the data from machine 2 which makes it difficult to compare with the other measurements. Even after the moving average filtration, the shape of the curve in Figure 22 shows a large variation between points which would indicate that the SLM shape would vary this much. This variation is not physically probable. A second measurement might have a smaller amount of noise and be a better indication of the actual shape of the SLM.

For machine 1, where the shape of the curves from the panel and camera data in Figure 22 looked quite similar, the difference between the camera range and the panel range is not that much. Taking into account the fact that the panel data only consists of 25 points and could therefore have missed variations that were not missed by the camera data, the camera data seems to give an accurate view of how the focus error changes over the length of the SLM image for this machine.

The data from the Fraunhofer Institute cannot be seen to correlate to either the panel or the camera data. This could in part be as a consequence of the fact that the camera and panel data are recorded with all of the optical aberrations included in the data, whereas the data from the Fraunhofer Institute have most of the optical aberrations from their optical system eliminated from their data. Another observation is the fact that the shape for the two SLM chips is very flat for most of the length of the SLM. This could indicate that the measurements from the camera and the panel are only picking up errors from the optical system. The original focus errors at the panel were never checked to see if they showed any resemblance to the data from the Fraunhofer Institute.

Measurement of p_1 planarity

The p_1 planarity refers to the displacement error in the x-direction, as seen in Figure 7. This displacement can be seen as a shift in the peak location of the Gaussian illumination that exists on the short direction of the SLM. By measuring this peak movement the p_1 parameter can be determined.

The twist in the SLM will reflect light at different angles along the length of the SLM. Since the SLM image is set at a distance z_{illum} from the illuminator focus, as shown in Figure 10, the different angles will lead to a shift in the image at the panel. A schematic of this shift at the panel is shown in Figure 24.

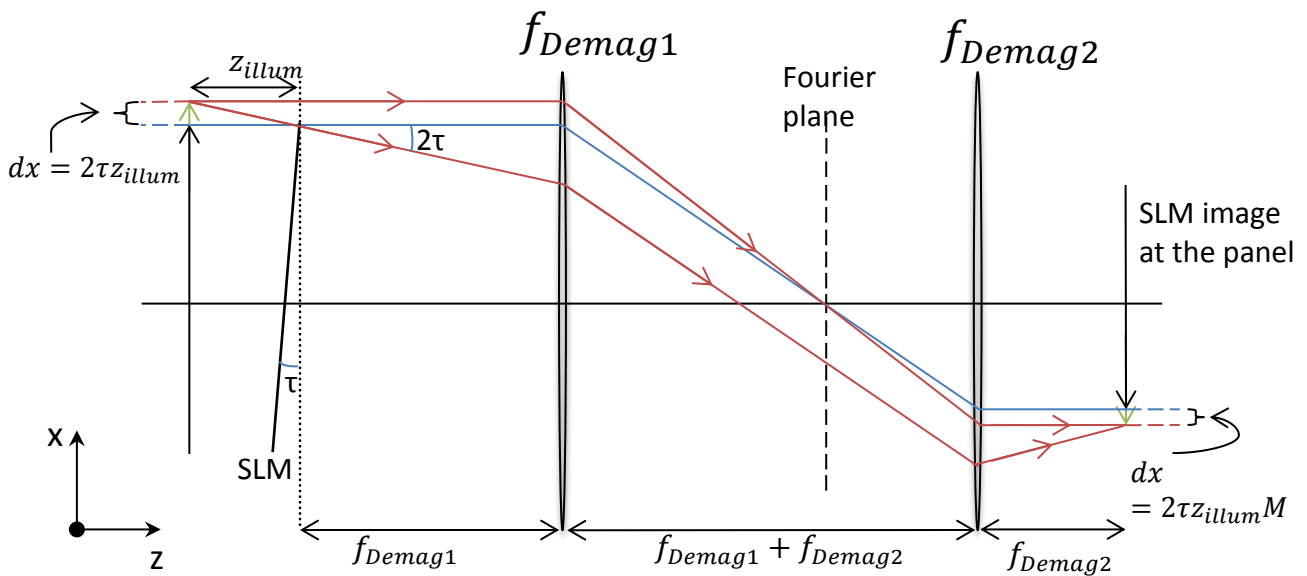


Figure 24 – A sketch showing how the SLM is imaged in the x-direction and how a SLM with a tilt in the x-direction will give a displacement error at the panel.

The schematic in Figure 24 shows that the SLM image is placed at a distance z_{illum} from the illuminator focus. This means that the image of the SLM image is traced from a distance of $f_{Demag1} + z_{illum}$ behind the first lens, while the SLM chip is placed at a distance f_{Demag1} behind the first lens. The twist in the SLM is measured as the angle τ that the SLM makes with the x-axis. This angle will lead to a displacement in the x-direction in the final image $dx = 2\tau z_{illum} M$. This displacement will be exaggerated as the image is moved from the focal point f_{Demag1} along the z-axis, i.e. out of focus. This exaggeration is described by Figure 25.

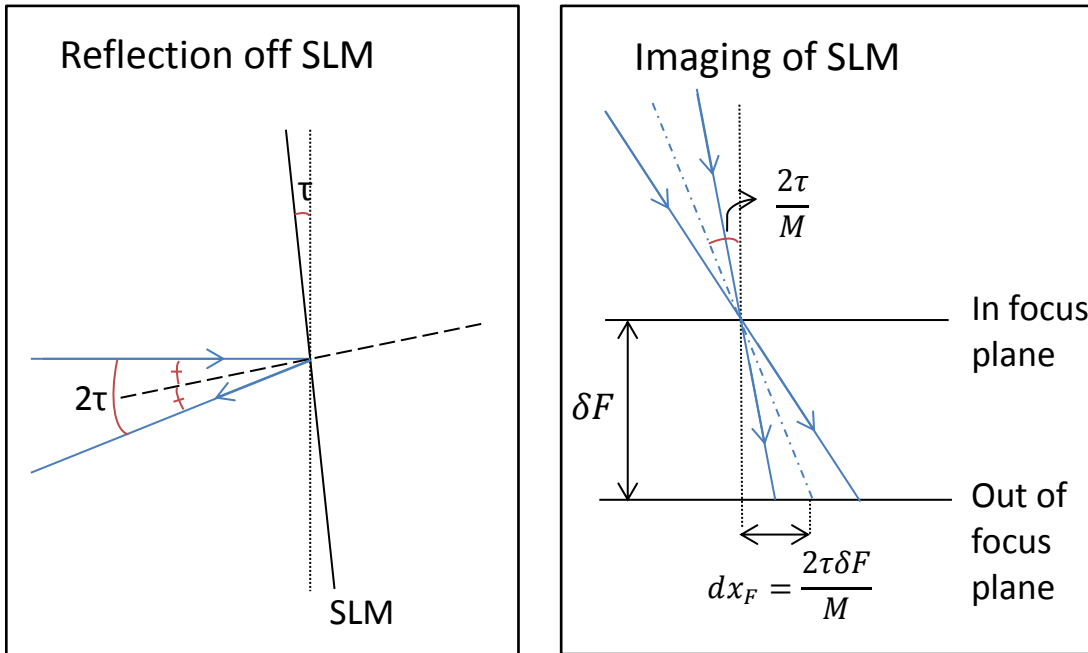


Figure 25 – The sketch to the left shows how a SLM tilted with an angle τ will be reflected with an angle 2τ . The sketch on the right shows how the displacement error at the panel will be exaggerated in an out of focus plane due to the landing angle that the tilt of the SLM in the x-direction will contribute to.

The reflection from the SLM will give an angle of 2τ from the incoming beam to the reflected beam as can be seen in the first sketch of Figure 25. This angle will be rescaled to $\frac{2\tau}{M}$ in the image plane labeled as the “in focus” plane in the second sketch in Figure 25. This second sketch shows that the SLM image will be focused to a point in the “in focus” plane. When the image is moved δF to the “out of focus” plane, the displacement dx_F will be $\frac{2\tau\delta F}{M}$. The SLM contribution to the total displacement error is then given by:

$$dx_{tot} = dx + dx_F = 2\tau z_{illum}M + \frac{2\tau\delta F}{M} \quad (4)$$

Experiment

Images were taken at $100\mu\text{m}$ steps in the positive and negative z-direction from the best focus position using the same camera as for the p_2 planarity measurements. Images containing the pulse pattern were also taken to be able to identify the pixel at which the images should be stitched together. Background images were taken to reduce noise. The SLM images were analyzed in a similar way as those taken to image the p_2 planarity of the SLM. These images were taken on the same two machines as for the p_2 planarity measurements.

Image Analysis

Once again the whole SLM image did not fit into one camera frame and therefore three images were taken at each z-position of the camera. The three images were cropped and rotated individually after the background noise had been subtracted. The pulse pattern was again utilized to identify the edge pixels of the SLM in the images and the analysis was done from

half way up the taper as in Figure 14. Each of the three images was then fit with a Gaussian fit as in Figure 15 and the location of the peak was now recorded. Plots were made showing the peak movement along the length of the SLM. These plots were stitched together at the stitch positions given by the pulse pattern and the final plot of the peak movement for one of the machines is shown in Figure 26.

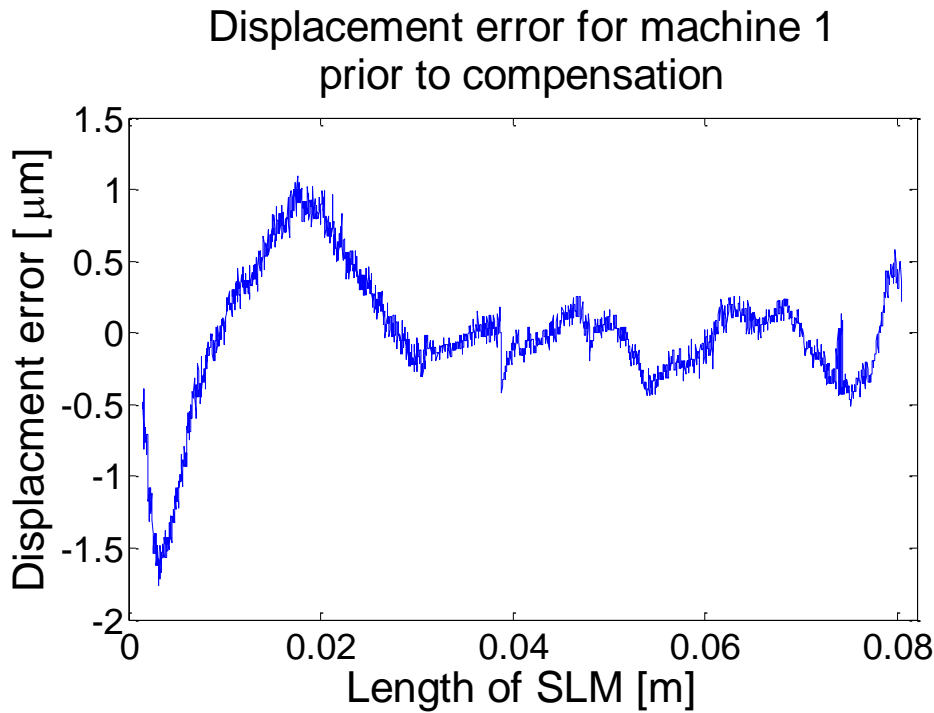


Figure 26 – In focus displacement error measurements from machine 1 prior to compensation.

As for the p_2 measurements, the plot in Figure 26 has some noise present. To reduce this noise, the data from the plot was sent through a moving average filter taking the average of the 20 points closest to every point. The resulting plot after the moving average filtration is shown in Figure 27.

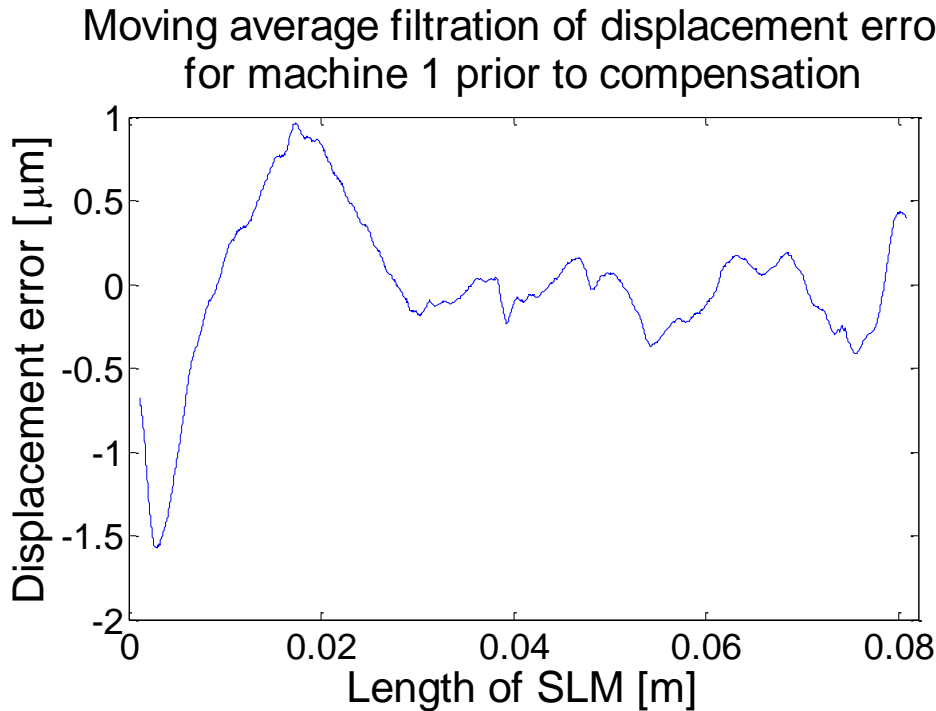


Figure 27 – The displacement error from machine 1 prior to compensation once it has passed through a moving average filter to reduce noise.

The error was calculated for the data in Figure 27 in the same way as for the measurements for the p_2 planarity measurements, using Monte Carlo simulations. For this data 1000 peak values were generated from the 1000 intensity values in the Gaussian fit in Figure 15. These 1000 peak values gave an error of $\pm 0,011\mu\text{m}$. This value is less than one percent of the range of the measured values and the error bars were not visible in the plot and have therefore not been included in the plot in Figure 27. The full code used to do this analysis can be found in [8].

Results and Analysis

The results from the two machines are displayed in the plots below along with the Fraunhofer data and the panel data. The panel data and the camera data have once again recorded all of the optical aberrations as well as the displacement error due to the twist of the SLM surface. The panel data has traveled through more optics than the camera data and so has more aberrations included in the collected data. As in the previous measurements of the p_2 planarity, the camera data and the Fraunhofer data consists of around 3500 points whereas the panel data consists of 25 points.

Comparison of displacement error measurements for machine 1 prior to compensation

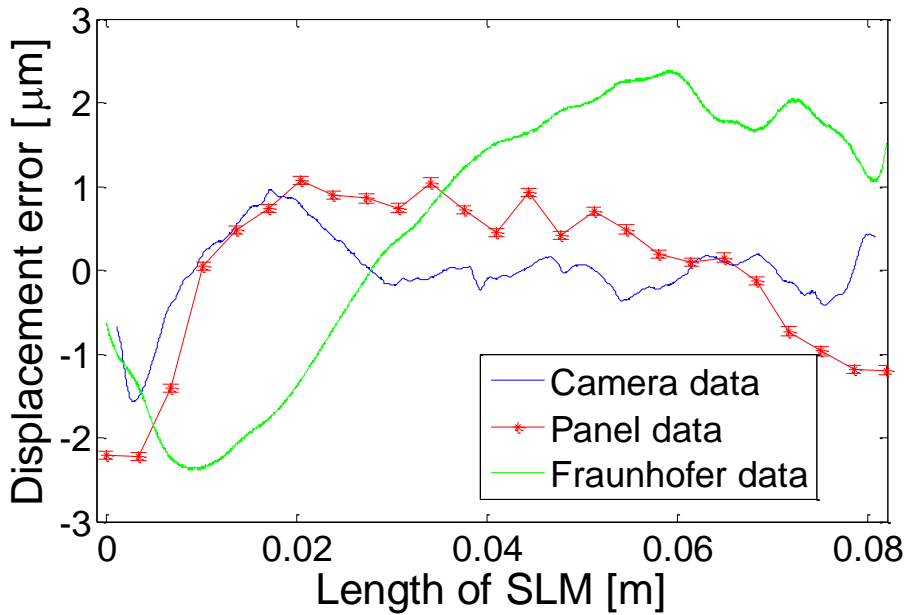


Figure 28 – A plot comparing the displacement error from machine 1 prior to compensation from the data collected in the camera, at the panel and at the Fraunhofer Institute.

Comparison of displacement error measurements for machine 2 prior to compensation

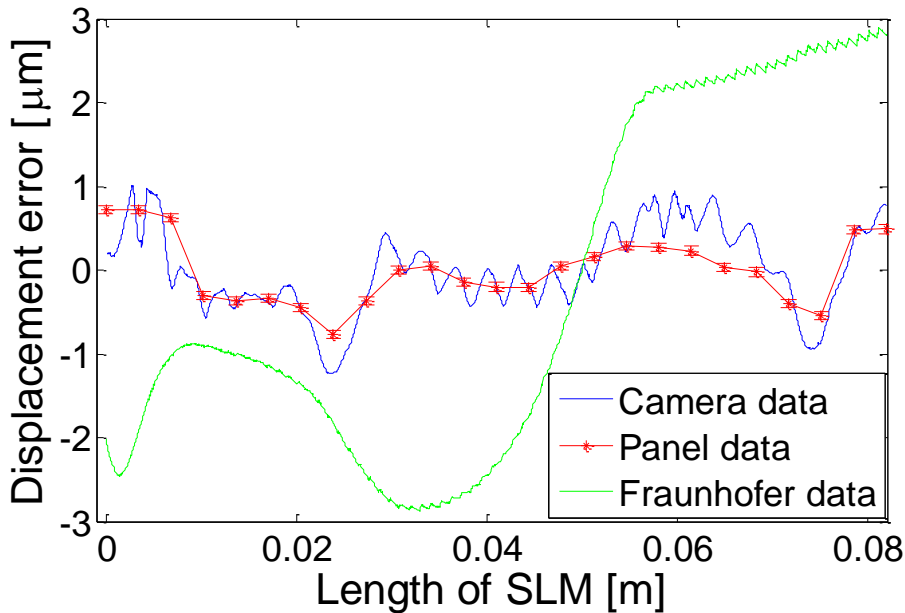


Figure 29 – A plot comparing the displacement error from machine 2 prior to compensation from the data collected in the camera, at the panel and at the Fraunhofer Institute.

Figure 28 and Figure 29 represent data for the displacement error when in focus prior to the machine compensation of the displacement error. To see what the specification is for the displacement error after compensation, see the acceptance values in [9]. The data from the panel and the camera have been taken for the same focus position.

The plot in Figure 28 has a good correlation between the panel data and the camera data. The same good correlation can be seen in the data for machine 2 displayed in Figure 29. The Fraunhofer data for machine 1 can be seen to show a resemblance to the shape of the camera and panel data, but the range is larger in this case. The Fraunhofer data for machine 2 on the other hand cannot be seen to exhibit the same shape as the panel or camera data for machine 2. The ranges of all the data for the displacement have been collected into Table 2.

	Machine 1	Machine 2
Camera data	2,54 ±0,011	2,25 ±0,011
Panel data	3,29 ±0,005	1,49 ±0,005
Fraunhofer data	4,77	5,74

Table 2 – A table summarizing the p_1 data from the two machines prior to compensation.

For machine 1 the camera has a range 30% smaller than the range for the panel data. The Fraunhofer data has a range 50% larger than the camera data. For machine 2 the camera data has a range 50% larger than the panel data and the Fraunhofer data is more than double the range of the camera data. The measurements from machine 2 have once again a larger amount of noise than the measurements from machine 1. This could be a reason why the range of the camera data in machine 2 is so much larger than the panel data compared to the data from machine 2. The variations in the measurements from the camera and panel data could be as a consequence of the extra optics that the panel data traverses just as for the measurements on the p_2 planarity.

As seen from the results for the p_2 planarity, there is no one plane at which the whole SLM is in focus. The p_1 planarity contributes to a different displacement error when out of focus and when in focus. This implies that the displacement error in some places of the camera data should be scaled as out-of-focus displacement error while others should be scaled as in-focus displacement error. The plots, Figure 28 and Figure 29, have only been taken to be in-focus errors. Since the Fraunhofer measurements are done in focus for the whole length of the SLM, the comparison made in these plots to the Fraunhofer data is not completely correct.

This along with the fact that the optical errors were not compensated for could explain the deviation in the data sets for Figure 28. For the results from machine 2, more investigation needs to be done as to why the shapes differ so much.

Out of focus displacement error for machine 1 prior to compensation

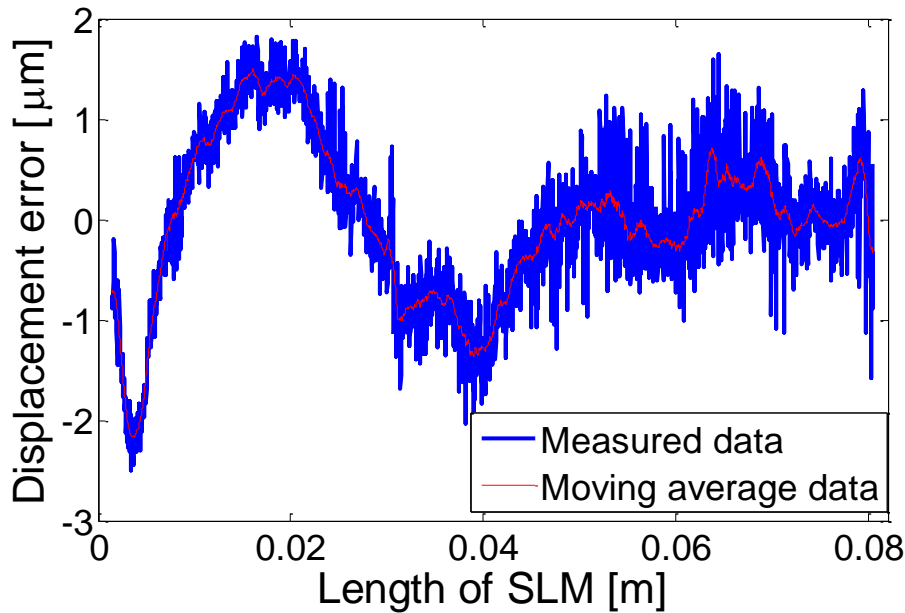


Figure 30 – Out of focus displacement error for machine 1 prior to compensation showing the increasing amount of noise present in the analyzed data.

The data in Figure 30 shows the data for one image taken 400 µm out of focus. The moving average filtration does show quite a good representation off the measured data, but there is an amount of uncertainty as to its actual position where the noise is the highest, e.g. the end of the graph. The noise is due to the Gaussian fit in the code being bad. As the camera is moved out of focus, the Gaussian illumination during the experiments in this machine gets worse by the presence of a shoulder next to the illumination peak as well as the intensity decreases. The code for the image analysis then tries to fit a Gauss to a non-Gauss curve and makes the resulting plot very noisy.

The images that were taken out of focus were initially done because it was thought that a shift in peak of one pixel was needed to properly measure the displacement error. Since the analysis includes a Gaussian fit in the short direction, this was not necessary and therefore these images were not used to determine the displacement error.

Measurement of T planarity

As mentioned earlier in the background, the illumination on the SLM consists of a number of illuminator lines, each one illuminating the whole surface of the SLM. These lines will be imaged in the Fourier plane indicated in Figure 3. Since each line illuminates the whole SLM surface, every part of the SLM will see all of the illuminator lines. With a curvature in the long direction of the SLM, each part of the SLM will see and image the illuminator lines at a different angle. When the whole SLM is illuminated, these lines will appear slightly blurred because the image is a superposition of the contribution from all parts of the SLM. By illuminating a small portion of the SLM, the illuminator lines will be narrower. When the illuminated portion is changed, these lines will have shifted if the angle of the reflected light is changed, due to the curvature of the SLM in the long direction. This can be used to calculate the bow of the SLM in the long direction. The relation between the angle of the bow of the SLM in the long direction and the movement of the illuminator lines in the Fourier plane is shown schematically in Figure 31.

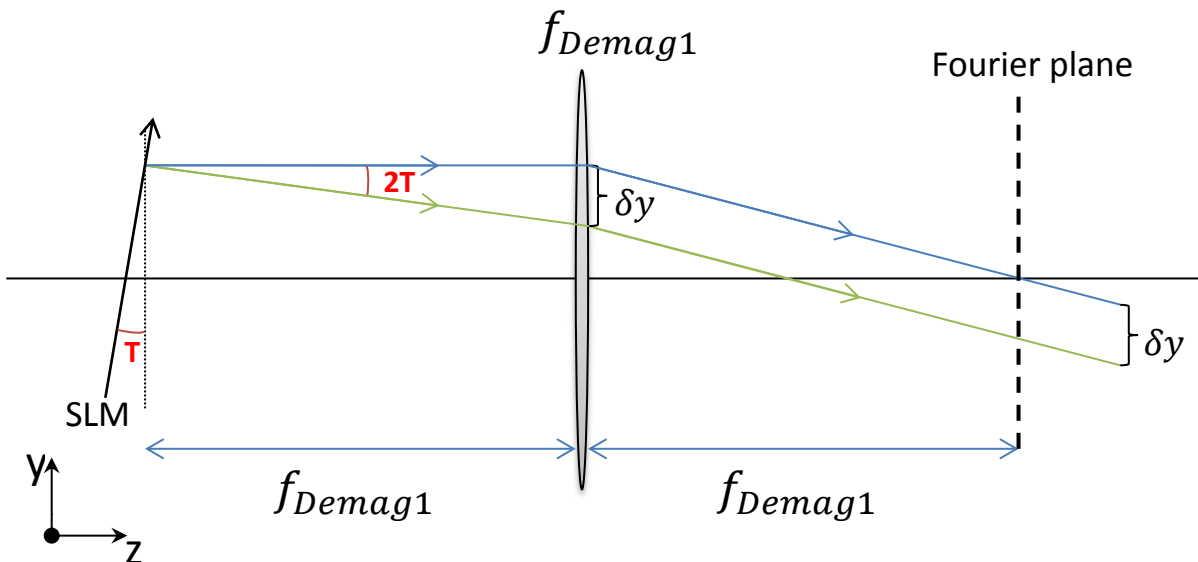


Figure 31 – A schematic view of how an angle in the SLM in the y-axis will move the illuminator lines in the Fourier plane.

Previously the SLM has been shown to be placed at a distance z_{illum} from the illuminator focus, Figure 24. This is true for the x-direction of the SLM. However, in the y-direction the SLM is placed in the illuminator focus. This difference in focus for the x- and y-directions is achieved with a cylindrical lens prior to the SLM which separates the focus in the two directions by a distance z_{illum} .

Since the SLM is placed in the illuminator focus in the y-direction, the bow of the SLM will not contribute to a displacement error at the panel when the machine is writing in focus. This bow will only give a displacement error once the machine starts writing out of focus due to the landing angle that the bow will give. This is the same as the landing angle sketched in Figure 25 for the p_1 planarity, where τ has now been replaced by T .

Just as for the p_1 planarity, if the SLM is tilted by an angle T , the reflected light will be reflected at an angle $2T$. Since the SLM is placed in the focal point of the lens, all rays

emerging from the SLM will be parallel after they have been transmitted by the lens. This leads to a simple expression for the movement of the illuminator lines and the angle T that describes the bow of the SLM in the long direction.

$$\delta y \cong 2T * f_{Demag1} \quad (5)$$

The angle T shown in Figure 31, is the same angle that is shown in Figure 8. δy is the distance the illuminator lines will shift due to the angle T in the SLM. f_{Demag1} is the focal length of the lens in the image.

Fourier Lens Design

To be able to image the Fourier plane onto the existing in machine camera, a lens needed to be inserted into the machine. The properties of this lens are described below.

The rays emerging from the optical system in Figure 3 will give an image of the Fourier plane at infinity, i.e. parallel rays. The lens that needs to be inserted to image the Fourier plane onto the camera, position of panel in Figure 3, will then be placed between the second lens and the image plane (camera plane). The distance between the Fourier lens, lens to be inserted, and the image plane will be equal to the focal distance of the Fourier lens. This new optical system is shown schematically in Figure 32.

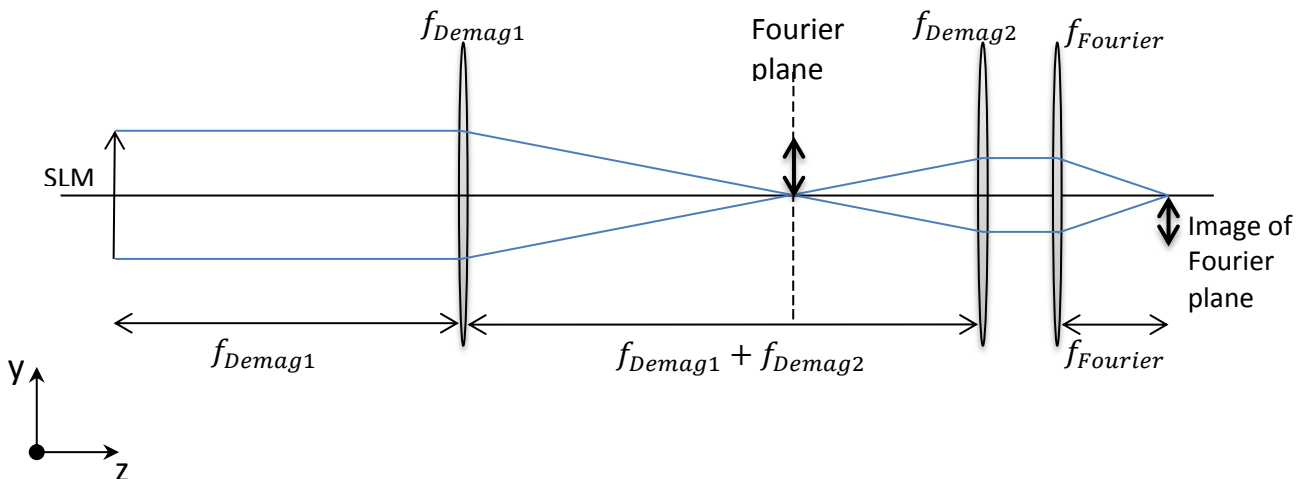


Figure 32 - A schematic of the optical system with the Fourier lens inserted moving the image of the Fourier plane from infinity to the camera plane.

With the Fourier lens in place the movement of the lines in the Fourier plane will be rescaled by the magnification factor of the two lenses f_{Demag2} and $f_{Fourier}$. The new relation between the movement of the lines and the angle T will be as in equation (6) below.

$$\delta y \cong 2T * f_{Demag1} * \left(\frac{f_{Fourier}}{f_{Demag2}} \right) \quad (6)$$

This equation is the same as the one presented in equation (4), but simply scaled by the magnification factor $\left(\frac{f_{Fourier}}{f_{Demag2}} \right)$. The calculations for this lens can be found in [10].

Note: *The optical system of the machine has changed design from the old model to the current model. In the current model, the optical system is more compact and leaves little room to insert an extra lens. Since this lens could not be inserted without a small amount of rearranging in the machine, this experiment was performed on the older model where there was more space and no one else was using it at the time. All of the previous experiments have been performed on the current model. The magnification factor from the SLM to the panel is the same as in the current model. However, the magnification from the SLM to the camera plane is no longer the same value. This means that the magnification factor from the camera plane to the panel is no longer one. This only changes the value of M in the calculations.*

Experiment and Results

The lens was inserted into the machine so that the Fourier plane was imaged onto the camera. The first picture was taken with 6.25% of the pixels set to “white”. This means that these 6.25% of the pixels were set to transmit as much light as possible to the camera sensor. The rest of the SLM pixels (93.75%) were tilted “black”, i.e. they were tilted so that as little light as possible was transmitted to the camera sensor. The region of white pixels was moved downwards along the SLM with a step of 1.6% of the SLM length between each picture. The SLM pixels that are tilted “black” will still reflect some light at an angle that will transmit it through the optical system. Therefore a picture was taken with all of the SLM pixels tilted “black” to remove both the stray light from the SLM and any background noise.

The SLM was then removed from the machine and a planar mirror put in its place. A slit that was 5.1mm wide was placed in front of the SLM and moved along the length of the SLM with approximately 1.2mm increments. A picture was taken for every slit position. This gave a total of 61 images, the same amount recorded with the SLM in place. A background image was taken to eliminate noise.

Image Analysis

The images were again analyzed in MATLAB. The background image was subtracted from the images of the Fourier plane taken with the SLM present in the machine and one of the images is shown in Figure 33.

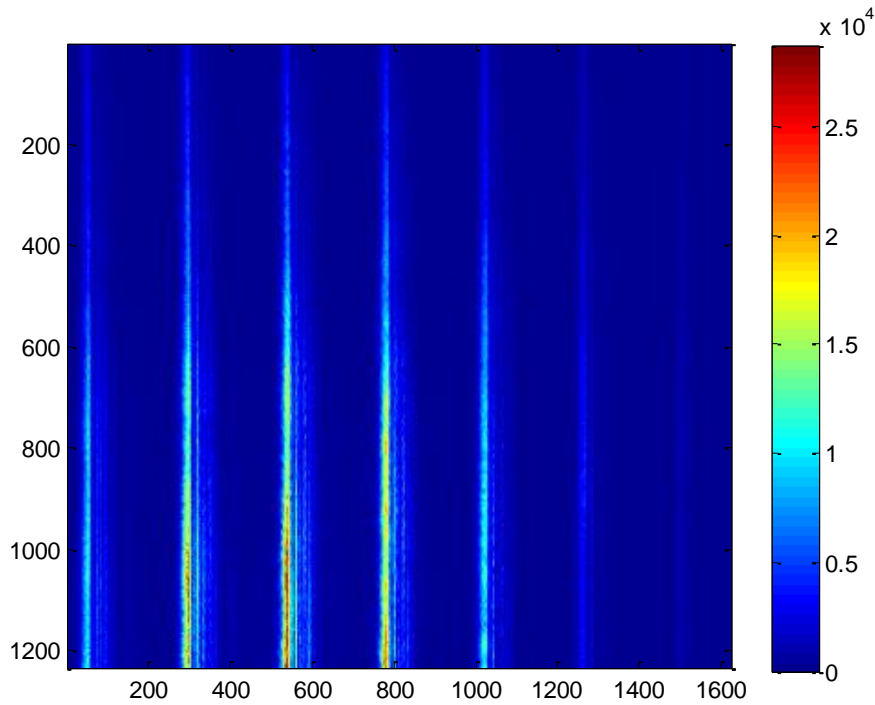


Figure 33 – Image of the Fourier plane showing the illuminator lines when one portion of the SLM is illuminated.

In Figure 33, a total of seven illuminator lines can be seen. The lines with the highest intensity represent the location of the illuminator lines for that portion of the SLM. There are a few lines of lower intensity close to the illuminator lines. These are reflections in the system and can be ignored for these measurement purposes. The position of the illuminator lines are picked out of the profile of the image in Figure 33. The profile is shown in Figure 34.

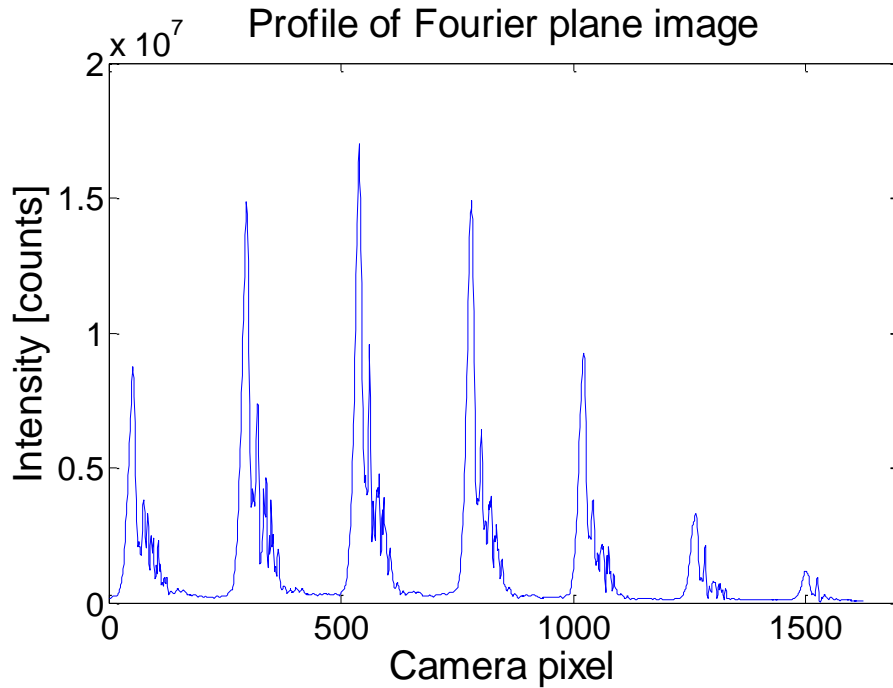


Figure 34 – Profile of the image displayed in Figure 33 that is used to determine the camera pixel position of the lines in each image.

The position of the seven peaks in each image was recorded. The distance that each line moved from image to image differed slightly for all of the seven lines. Since the distance between the lines should be constant, the movement of each of the lines from image to image should be the same for all of the seven lines. This slight difference in line movement could be a result of noise or camera pixel deviations where some pixels have a higher response than others. To get a more accurate representation of the line movement, the average line movement for all seven lines was taken and the resulting plot is shown in Figure 35.

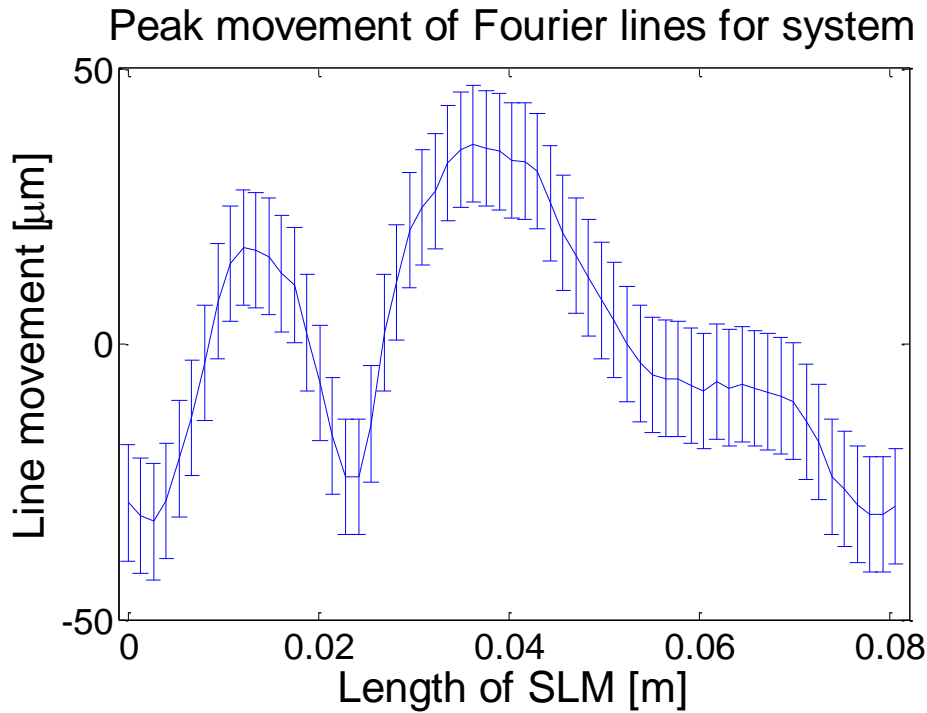


Figure 35 – A graph showing the movement of the illuminator lines along the length of the SLM in the camera plane.

The plot in Figure 35 shows how the Fourier lines moved along the length of the SLM along with the approximated error. This error was calculated by taking the standard deviation of the seven line movements and multiplying by six to get the full interval. The error bars therefore show a value of $\pm 10.5\mu\text{m}$ ($\pm 3\sigma$).

The same analysis was made for the images taken with a mirror in place of the SLM. The mirror should have a very flat surface with a variation in global planarity much smaller than the SLM surface. This means that the movement of the lines should only be caused by optical aberrations in the system. The movement of these lines was also recorded and the resulting plot is shown in Figure 36 below.

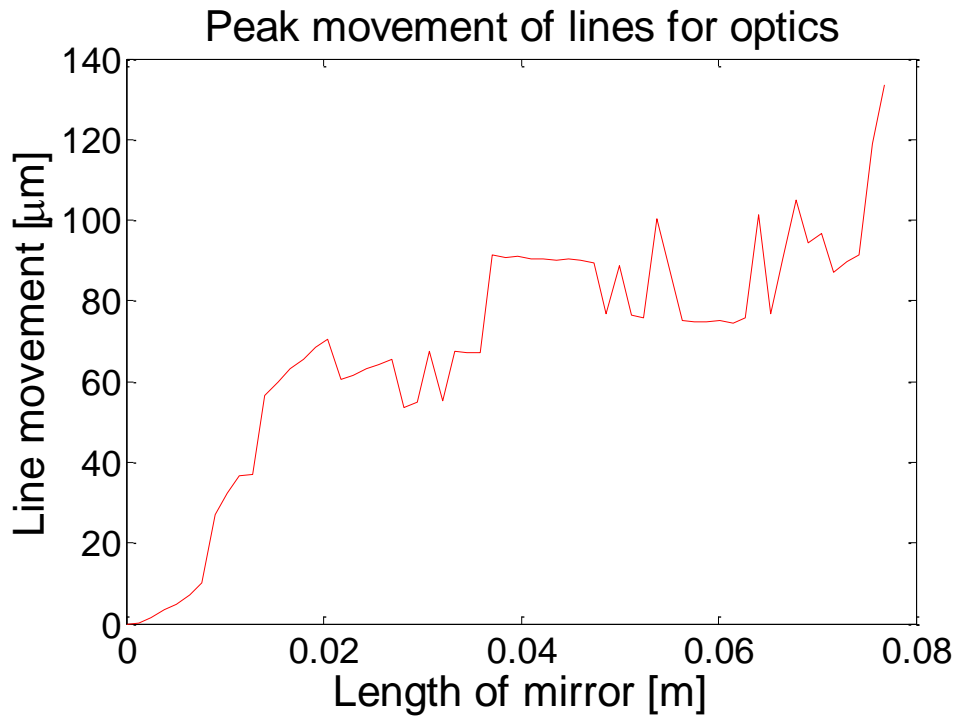


Figure 36 – Movement of Fourier lines for the optical system.

The plot shows a linear upward trend. This trend is due to the fact that the machine was set up to compensate for a spherical curvature of the SLM in the long direction. This curvature will be present as a linear movement of the lines for a plane mirror. The remaining movement of the lines after the linear tilt has been removed is shown in Figure 37.

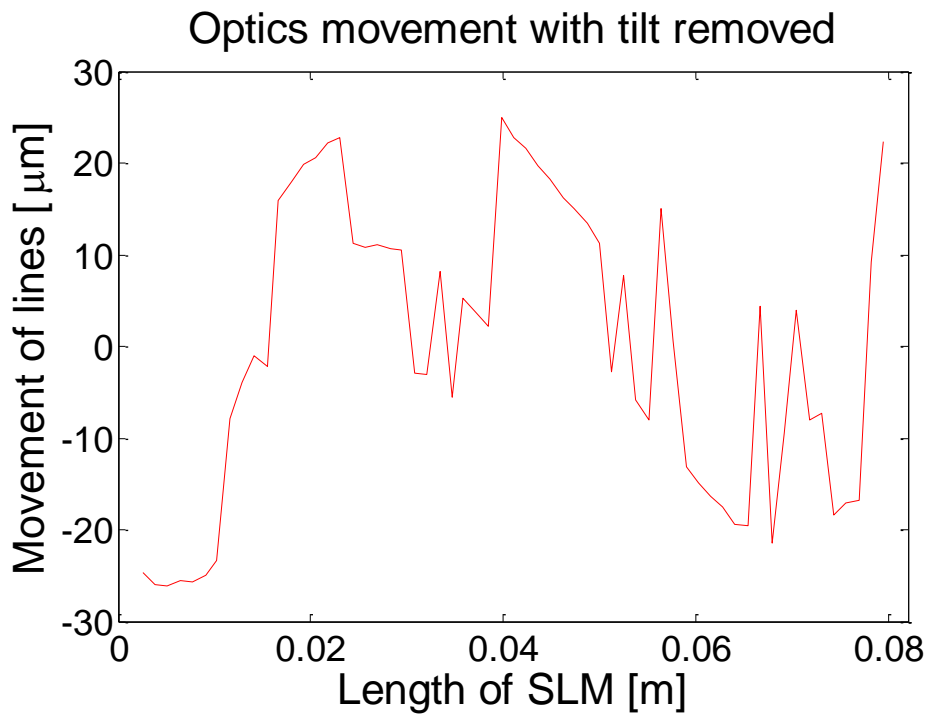


Figure 37 - The movement of the Fourier lines for the optical system with the tilt removed.

The movement of the lines in the figure above is due to the aberrations present in the optics.

The uncertainty of the movement in the x-direction is due to the uncertainty of the measurement instrument used to move the slit in 1.2mm increments. This uncertainty was estimated to be $\pm 0.05\text{mm}$. The error bars were too small and are therefore not shown in Figure 37.

To see what type of error the SLM is contributing to, this optical error in Figure 37 is subtracted from Figure 35 and the resulting plot is shown in Figure 38.

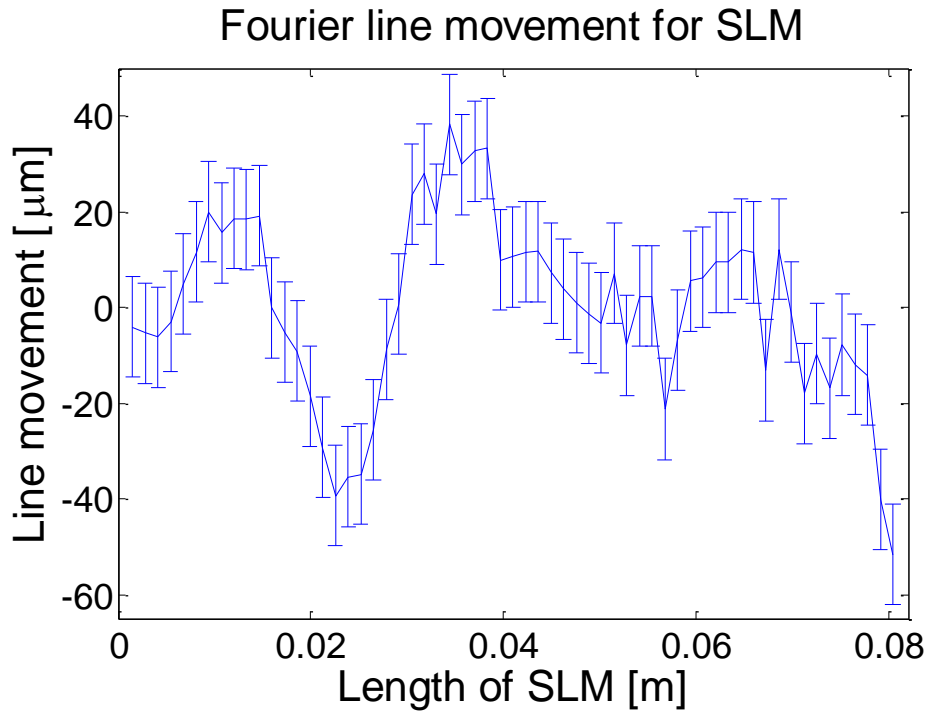


Figure 38 – The movement of the Fourier lines from the camera with the optics movement removed.

The plot in Figure 38 shows the movement of the Fourier lines when the optical aberrations have been compensated for with an uncertainty in the y-direction from the spread of the line movements for the SLM. The full code used to do this analysis can be found in [11].

Analysis

In the previous two measurements of the p_1 and p_2 planarity a comparison has been made of the data collected from the camera to data collected from both the panel and from the Fraunhofer Institute. Unlike the displacement error in the x-direction due to the twist of the SLM which will give a displacement error both in and out of focus, the bow in the long direction of the SLM will only give a displacement error when the machine is writing out of focus. A measurement of the displacement error in the y-direction at the panel was never made on the older model and therefore no such data comparison can be made with panel data. A comparison of the camera data and the Fraunhofer data can still be made and is shown in Figure 39. To be able to compare the two measurements properly, the camera data from Figure 38 has been rescaled to radians using equation (6).

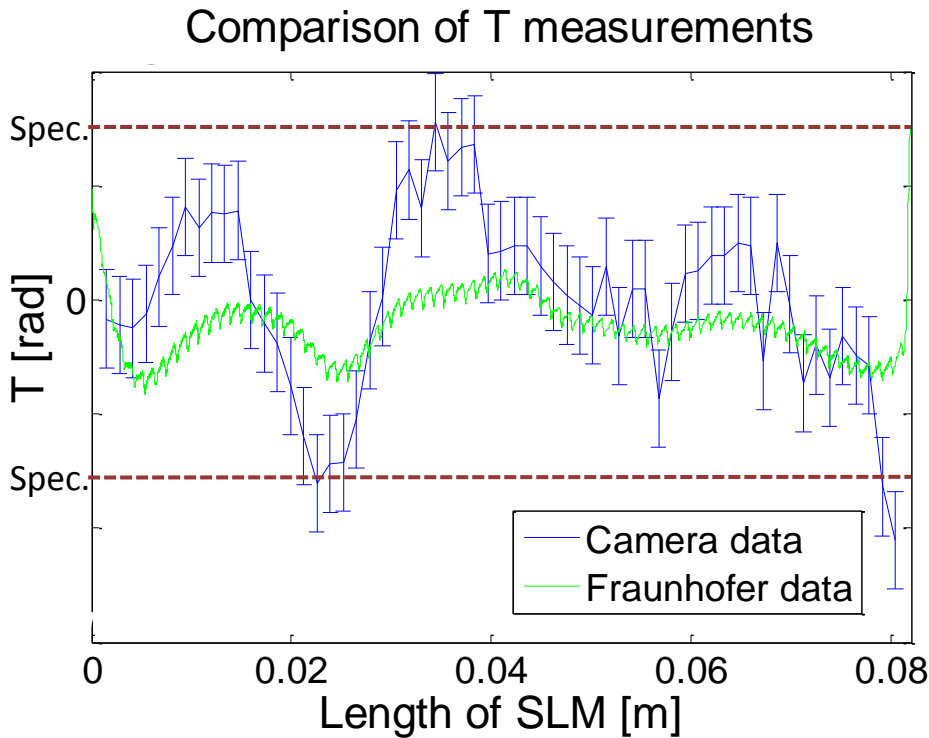


Figure 39 – Comparison of T data from the Fraunhofer Institute and the camera.

Again, due to non-disclosure of confidential information the values on the y-axis in Figure 39 are not shown. The two specification limit lines are shown for analysis. For specification values see the acceptance values in [9].

The camera data here consists of 61 data points whereas the Fraunhofer data consists of around 3500 points. This means that a variation of the bow in the long direction in an area smaller than 1.6% of the SLM size will be missed in the camera data.

Even though the camera data points are much fewer, the camera data varies more than the Fraunhofer data. In Table 3, a similar comparison as to what was made for the p_2 ranges in Table 1 has been made. The table shows how much the data ranges differ from the specification limit. The range of the Fraunhofer data has been taken for approximately the same parts of the SLM that the camera was analyzed for.

	T-range
Camera data	+20% ±15%
Fraunhofer data	-62%

Table 3 – Comparison of range for T data from the Fraunhofer Institute and the camera data.

Table 3 shows that the camera data exceeds the specification limit by 20%. The machine that these measurements were done on had not been used for over six months. The writing quality of this machine could therefore not be verified and it is possible that the machine could no longer write within specifications without any realignment or other alterations. The uncertainty

of the Fraunhofer data can again be taken to be much smaller than the variation of T along the SLM length.

Since this measurement could not be done on any other machine it is difficult to say whether this planarity can be measured properly using a camera. More measurements on other systems where the optical aberrations have been measured would give a better indication as to whether this is a good method.

To be taken into consideration as to the reliability of this result is that when finding the right distance to move the camera to find the point where the Fourier plane was in focus on the camera was quite difficult. The lines should be wider when out of focus and thinner when in focus but the point at which the best focus was achieved was not easily detected on the camera. This could exaggerate the line movement in the final plot and it is possible that the range of the T values actually are smaller considering that the images were probably taken out of focus.

The result of the measurement of the optics contribution to the line movement showed a movement of around $50\mu\text{m}$ compared to the line movement of the whole system of around $100\mu\text{m}$. This movement from the optics is quite large and had a large impact on the resulting plot of the line movement of the SLM in Figure 38. This indicates that a measurement of the optical aberrations in the machines that p_1 and p_2 were measured in might also change their resulting curves significantly and possibly make them resemble the measurements from the Fraunhofer Institute more.

Conclusion and Future Work

The aim of this project was to try to determine if the planarity of the SLM chip could be measured with the current in-machine camera. From the experiments that have been made, it seems as though this is possible for the p_1 and p_2 planarity but could be difficult to determine for the T planarity without more experiments.

The p_1 and p_2 data did show a good correlation with the data that was measured at the panel. The camera can therefore provide a method to measure the SLMs global planarity with a higher resolution along the long direction of the SLM compared to the measurements done using the panel, from 25 data points to approximately 3200 data points.

These two data sets do include all of the optical aberrations from the whole optical train, but these are supposed to be small relative to the variations on the SLM surface. By characterizing the optical system with a plane mirror, this statement could be investigated and a more accurate result of the planarity of the SLM can be obtained. If this is necessary to be able to image the planarities, then a new optical characterization will be needed after each re-alignment of the system. Especially for the p_2 planarity which gives a focus error. This would be an inconvenience since this would require a removal of the SLM.

The measurements of the T planarity showed a very different shape than the one previously measured by the Fraunhofer Institute. With only one measurement, it is difficult to say whether this is a good way to measure this planarity. A lens to image the Fourier plane would have to be designed so that it could fit into the current model for more measurements to be possible. As mentioned earlier, it was not possible to fit a lens into the current model with ease due to a limited amount of space. Due to the small amount of space available it might not be possible to fit a lens in without altering some of the existing components, for example the camera might be moved higher up and then a lens might fit.

References

- [1] P. Askebjør, Trade off between Global flatness and Power durability of the LDI-SLM, Micronic Mydata Internal Report, SmarTeam: AB34072, 2012-12-03.
- [2] A. Karawajczyk, LDI projection optics technical description, Micronic Mydata Internal Report, SmarTeam: AB29861, 2012-06-05.
- [3] Datasheet Ceramic Substrate, Micronic Mydata Internal Report, SmarTeam: AB34506, 2013-06-12.
- [4] J. Heber et al., Contrast properties of spatial light modulators for microlithography, 673035, (2007), Proc. of SPIE Vol. 6730.
- [5] A. Svensson, TD - Reflex based calibration in LDI, Micronic Mydata Internal Report, SmarTeam: AB34509, 2013.
- [6] U.A.Dauderstädt M. Eckert, Description of global planarity spec LDI SLM, Micronic Mydata Internal Report, SmarTeam: AB34450, 2013-06-10.
- [7] E. Hecht, Optics, Second Edition, p.135-145: ISBN: 0-201-11611-1, 1987.
- [8] H. Al-Maawali, LDI SLM global planarity p1 p2, Micronic Mydata Internal Report, SmarTeam: AB34410, 2013-06-07.
- [9] P. Björnängen, SLM LDI specification, Micronic Mydata Internal Report, SmarTeam: AB34451, 2013-06-10.
- [10] H. Al-Maawali, R1 laser to plate 1.0 f including fourier lens, Micronic Mydata Internal Report, SmarTeam: AB34413, 2013-06-07.
- [11] H. Al-Maawali, LDI SLM global planarity T, Micronic Mydata Internal Report, SmarTeam: AB34411, 2013-06-07.